R-05-87

Rock mechanics characterisation of the rock mass – theoretical approach

Preliminary site description
Simpevarp subarea version 1.2

Anders Fredriksson, Isabelle Olofsson

Golder Associates AB

October 2006

SKB

Rock mechanics characterisation of the rock mass – theoretical approach

Preliminary site description Simpevarp subarea version 1.2

Anders Fredriksson, Isabelle Olofsson

Golder Associates AB

October 2006

Symbols and abbreviations

c_i Cohesion of intact rock [MPa]

c_f Peak cohesion of fracture [MPa]

c_m Peak cohesion of the rock mass, Mohr-Coulomb [MPa]

E_i Young's modulus of the intact rock [GPa]

E_m Young's modulus of the rock mass [GPa]

K_n Joint normal stiffness at expected normal stress [MPa/m]

K_s Joint shear stiffness at expected normal stress [MPa/m]

k_r Exponent in Power Law size distribution

T_i Tensile strength of intact rock[MPa]

UCS_i Uniaxial compressive strength of intact rock [MPa]

X_0 Minimum radius in Power Law size distribution

φ_i Internal friction angle of intact rock [°]

φ_f Internal friction angle of fracture, Mohe-Coulomb [°]

φ_m Internal friction angle of rock mass[°]

ν_i Poisson's ratio of the intact rock

ν_m Poisson's ratio of the rock mass

σ_1 Maximum principal in situ stress [MPa]

σ_2 Intermediate principal in situ stress [MPa]

σ_3 Minimum principal in situ stress [MPa]

σ_a Level of horizontal confining stress for simulations [MPa]

σ_b Level of horizontal confining stress for simulations [MPa]

σ_H Maximum horizontal in situ stress [MPa]

σ_h Minimum horizontal in situ stress [MPa]

σ_{vf} Vertical stress at failure [MPa]

Abstract

The present Report summarises the theoretical approach to estimate the mechanical properties of the rock mass in relation to the Preliminary Site Descriptive Modelling, Simpevarp subarea, version 1.2.

The theoretical approach is based on the geometrical DFN-description (Discrete Fracture Network) of the fracture system in the rock mass and on the results of mechanical testing of intact rock and on rock fractures from the site.

To estimate the mechanical properties of the rock mass a load test on a rock block with fractures is simulated with the numerical code 3DEC. The location and size of the fractures are given by DFN-realisations. The rock block is loaded in plain strain condition. From de calculated relationship between stresses and deformations the mechanical properties of the rock mass are determined.

The influence of the geometrical properties of the fracture system on the mechanical properties of the rock mass is analysed by loading 20 blocks based on different DFN-realisations. The material properties of the intact rock and the fractures are kept constant. The properties are set equal to the mean value of each measured material property.

The influence of the variation of the mechanical properties of the intact rock and variation of the mechanical properties of the fractures are estimated by analysing numerical load tests on one specific block (one DFN-realisation) with combinations of properties for intact rock and fractures. Each parameter is varied from its lowest values to its highest values while the rest of the parameters are held constant, equal to the mean value. The resulting distribution is expressed as a variation around the value determined with mean values on all parameters.

To estimate the resulting distribution of the mechanical properties of the rock mass a Monte Carlo simulation is performed by generating values from the two distributions, caused by fracture network variation and property variation, independent of each other. The two values are added and the statistical properties of the resulting distribution are determined.

Sammanfattning

Denna rapport sammanfattar det teoretiska angreppssättet att uppskatta bergmassans mekaniska egenskaper i samband med den platsbeskrivande modellen version 1.2 för Simpevarp

Det teoretiska angreppssättet baseras dels på den geometriska DFN-beskrivningen (Discrete Fracture Network) av bergmassans spricksystem och dels mekaniska laboratorietester utförda på intakt berg och på bergsprickor från platsen.

För att uppskatta bergmassans mekaniska egenskaper utförs ett numeriskt belastningsförsök på ett bergblock i den numeriska koden 3DEC. Läge och storlek på sprickorna i blocket baseras på DFN-realiseringar. Blocket belastas under plant töjningstillstånd.

Inverkan av spricksystemets geometriska utformning bestäms genom att analysera ca 20 st DFN-realiseringar med konstanta egenskaper hos det intakta berget och hos sprickorna. Egenskaperna har satts lika med de uppmätta medelvärdena för respektive egenskap.

Inverkan av variation hos det intakta bergets och sprickornas mekaniska egenskaper bestäms genom att för en DFN-realisering utföra analyser med kombinationer av egenskaper. Varje parameter varieras mellan dess lägsta och högsta värde medan övriga parametrar hålls konstanta. Den resulterande fördelningen uttrycks som variation kring det värde som bestämts med medelvärde på alla egenskaper.

För att erhålla den resulterande fördelningen på bergmassans egenskaper görs Monte-Carlo simuleringar där ett värde slumpas fram ur de bestämda fördelningarna över spricksystemets geometriska inverkan och inverkan av variation av delkomponenternas egenskaper. De två värdena adderas för att erhålla den resulterande fördelningen hos bergmassans mekaniska egenskaper.

Contents

1   Introduction

This work reports results from one of the four rock mechanics activities that have been recognised within the project "Simpevarp Area – Site Descriptive Model during the initial Site Investigation stage version 1.2". This activity aims to determine the undisturbed mechanical properties of the rock mass in the local model area for Simpevarp 1.2. These parameters will be used for the preliminary design and to evaluate the suitability of the site.

The approach used in this activity is based on numerical simulations with the use of the 3DEC software /3DEC 2003/. The methodology has been developed in the purpose of the Site Investigations and is built upon three different models: the DFN model which is used to simulate the fracture network in the rock mass, the 3DEC mechanical model which is used to calculate the rock mass mechanical properties, and the GoldSim model which is the tool for estimation of combined variabilities.

The modelling procedure is described in detail in /Olofsson and Fredriksson 2005/.

The DFN model, the in situ stresses as well as the mechanical properties of intact rock and fractures constitute the input data that are necessary to build the 3DEC model, and are described in Chapter 2. Then the set-up of the 3DEC model and the procedure used for numerical simulations are described in Chapter 3. The results obtained from simulations in 3DEC and GoldSim are reviewed and analysed in Chapter 4, and the summary tables of mechanical properties of the rock mass are presented. Chapters 5 and 6 present a short discussion and conclusions of the study.

2 Indata

2.1 Intact rock

In order to determine what intact rock parameters should be assigned to the material in a specific rock domain, the main and subordinate rock types were given with an estimation of their occurrence in each rock domain, Table 2-1. Regarding the composition of the rock domains and the rock types that have been tested values are available for rock domain A and B, called respectively RDA and RDB.

Laboratory test data are available only for two rock types, the quartz monzonite to monzodiorite and the fine-grained dioritoid, /Lanaro and Fredriksson 2005/.

2.2 Fractures

2.2.1 Geometry of fractures

The parameters for the DFN model used in this study (Simpevarp version 1.2) were delivered and presented at the end of June 2004. The statistical parameters are described in /LaPointe and Hermanson 2005/.

One alternative was developed which is based on six sub-vertical sets of fractures and one sub-horizontal set of fractures. Three of the sub-vertical sets (NNE-NE, EW-WNW and NW-NNW) are defined as regional and their characterisation (orientation, size distribution and intensity) is based on information from outcrops and lineaments. The other three sub-vertical sets (BGNE, BGNS and BGNW) are considered to represent the background fracturing in the rock mass and their characterisation is based on outcrop data.

Sub-horizontal fractures (SubHZ) are also considered to belong to the background fracturing of the rock mass but their characterisation is based only on borehole data.

The parameters for the DFN model have been studied and used for generating the 3D fracture network required for setting-up the numerical mechanical model. The parameters in the DFN model are presented below.

Table 2-1. Rock types identified in the different rock domains (from /Appendix 6, SKB 2005/).

Rock domain	Main rock type	%	Subordinate rock types	%
RDA	Ävrö granite	75.8–84.7	Fine- to medium- grained granite	0.8–21.5
			Fine-grained dioritoid	9–17
			Fine-grained mafic rock	3–4.9
RDB	Fine-grained dioritoid	90.6–94.2	Fine- to medium- grained granite	0.9–6.7
			Quartz monodiorite	0–3.5
RDC	Quartz monzodiorite	51.5–73.9	Fine-grained dioritoid	6.5
	Ävrö granite	22.9–34.1	Fine- to medium- grained granite	1.8–4.2
			Granite	2
RDD	Quartz monzodiorite	–	Fine- to medium- grained granite	–
			Pegmatite	–
			Fine-grained mafic rock	–

Orientation

The mean trend and plunge together with dispersion are given for each set disregarding if the fractures are open, partly open or closed (definition according to BOREMAP mapping). In Table 2-2 the parameters for the orientation of sub-vertical fracture sets are given and in Table 2-3 the parameters for the orientation of the sub-horizontal fracture set. The parameters for orientation of the fracture sets are equal in all rock domains A, B, C and D.

Size distribution

The size distributions used are the ones provided in the DFN model, Simpevarp version 1.2. Table 2-4 contains data for the sub-vertical sets and Table 2-5 for the sub-horizontal set. For numerical reasons in 3DEC only fractures with a radius larger than 1 m were generated. The parameters for size distribution for the fracture sets are equal in all rock domains A, B, C and D.

Table 2-2. Orientation of the sub-vertical fracture sets, from /LaPointe and Hermanson 2005/.

Orientation Set name	Mean pole trend/ plunge/dispersion[1]	Model/K-S[2]	Relative % of total population of sub- vertical fractures
NNE-NE	118.0/1.9/17.3	Fisher Not significant	18.99%
EW-WNW	17.1/7.3/11.2	Fisher Not significant	17.75%
NW-NNW	73.1/4.7/13.7	Fisher Not significant	22.50%
BGNE	326.3/5.5 K1:17.65 K2:18.14	Bivariate Fisher 0.041/45.4%	18.60%
BGNS	96.8/3.8/20.32	Fisher not significant	15.44%
BGNW	22.1/2.4 K1:5.36 K2: 6.66	Bivariate Fisher 0.051/61.3%	6.71%

[1] k for univariate distribution, k_1 and k_2 for bivariate distribution.

[2] Distribution model/Statistics for the Kolmogorov-Smirnov Goodness-of-fit test.

Table 2-3. Orientation of the sub-horizontal fracture set, from /LaPointe and Hermanson 2005/.

Orientation Set name	Mean pole trend/ plunge/dispersion	Model/K-S	Relative % of total population of sub- horizontal fractures
SubHZ	33/86/15	Selection by visual inspection, dispersion 15 degrees.	100%

Table 2-4. Size distribution for the sub-vertical fracture sets, from /LaPointe and Hermanson 2005/.

Size Set name	Model	Minimum size (X_0) (m)	k_r (parent population) or Std. deviation	Comments (used data etc)
NNE-NE	Powerlaw	0.36	2.58 (mass, median)	Estimated from outcrop data and lineaments.
EW-WNW	Powerlaw	0.36	2.8 (mass, median)	Estimated from outcrop data and lineaments
NW-NNW	Powerlaw	0.49	2.87 (mass, median)	Estimated from outcrop data and lineaments
BGNE	Log-normal	0.48	0.55	Estimated from outcrop data. Univariate Fisher also significant at 43.9% (K = 16.9)
BGNS	Log-normal	0.67	0.82	Estimated from outcrop data
BGNW	Log-normal	0.45	1.00	Estimated from outcrop data. Weakly-developed set; Bivariate normal also significant at 18.8%

Table 2-5. Size distribution for the sub-horizontal fracture set.

Size Model	Minimum size (X_0) or mean radius (m)	k_r (parent population) or Std. deviation	Comments (used data etc)
Lognormal	0.57	1.86	Estimated from borehole data (size from outcrop). Size model not well known (small data sample)

Intensity

Fracture intensity can be quantified by several measures, including the number of fractures per unit length (P_{10}), the number of fractures per unit area (P_{20}), the amount of trace length per unit area (P_{21}), and the amount of fracture surface area per unit volume of rock (P_{32}). The parameter P_{32} is often the most useful way to describe fracture intensity in a stochastic DFN model, as it is scale- and directionally-independent.

The tables provided for the DFN model v 1.2 /LaPointe and Hermanson 2005/ present intensities for sub-vertical sets and sub-horizontal sets for rock domains A, B and C (No information are provided for rock domain D). According to these tables the proportion (expressed in P_{32}) of sub-horizontal fractures in the rock mass is 30–37%. Nevertheless the proportion of sub-horizontal fractures in the rock mass is estimated from boreholes to be between 12 and 20% (respectively weighted and unweighted plots of fractures). Hence due to inconsistency of data the intensities of sub-vertical sets were re-calculated taking into account their relative proportion in the rock mass. The values of P_{32} are specific to rock domain, and for each rock domain the relative P_{32} for each fracture set was calculated, see Table 2-6 for rock domain A and Table 2-7 for rock domain B.

Table 2-6. P_{32} for all fracture sets in the rock domain A (RDA).

	All fractures		Open fractures		Sealed fractures	
P32 total	3.02		0.97		2.06	
% horizontal	12%	20%	12%	20%	12%	20%
NNE-NE	0.50	0.46	0.16	0.15	0.34	0.31
EW-WNW	0.47	0.43	0.15	0.14	0.32	0.29
NW-NNW	0.60	0.54	0.19	0.17	0.41	0.37
BGNE	0.49	0.45	0.16	0.14	0.34	0.31
BGNS	0.41	0.37	0.13	0.12	0.28	0.25
BGNW	0.18	0.16	0.06	0.05	0.12	0.11
SubHZ	0.36	0.60	0.12	0.19	0.25	0.41

Table 2-7. P_{32} for all fracture sets in the rock domain B (RDB).

	All fractures		Open fractures		Sealed fractures	
P32 total	7.66		1.42		6.24	
% horizontal	12%	20%	12%	20%	12%	20%
NNE-NE	1.28	1.16	0.24	0.22	1.04	0.95
EW-WNW	1.20	1.09	0.22	0.20	0.97	0.89
NW-NNW	1.52	1.38	0.28	0.26	1.24	1.12
BGNE	1.25	1.14	0.23	0.21	1.02	0.93
BGNS	1.04	0.95	0.19	0.18	0.85	0.77
BGNW	0.45	0.41	0.08	0.08	0.37	0.33
SubHZ	0.92	1.53	0.17	0.28	0.75	1.25

The P_{32} given in Table 2-6 and Table 2-7 represents the mean fracture intensity of the fracture network in the given rock domains. The fracture intensity actually varies inside the rock domains but this is neither described nor analysed in this report.

2.2.2 Mechanical properties of fractures

Laboratory normal load tests up to 10 MPa and shear tests at the different normal stress levels, 0.5, 5 and 20 MPa have been performed on fractures from borehole KSH01A, KSH02A and KAV01. The laboratory tests are evaluated and the results given by /Lanaro and Fredriksson 2005/.

The data was statistical analysed. A truncated normal distributed was chosen by expert judgement to describe the model. The preliminary mechanical properties of fractures that were used at this stage is presented in Table 2-8 in terms of mean, span and range of potential values for each parameter. The cohesion is expressed as a function of the friction angle as the two parameters are correlated.

Table 2-8. Summary of mechanical properties of fractures evaluated from laboratory tests /Lanaro and Fredriksson 2005/.

Parameter for single fractures (small scale).	All fracture set [1] Truncated normal distribution mean/standard deviation;	Min trunc. – max trunc.
Normal stiffness	100/32 MPa/mm	49–179 MPa/mm
Shear stiffness	29/11 MPa/mm	10–49 MPa/mm
Peak friction angle, φ	32°/4°	24°–40°
Cohesion [2]	$c_{mean} = 2.35–0.058 \cdot φ/0.25$ MPa	$c_{min} = c_{mean} – 0.37$ MPa
		$c_{max} = c_{mean} + 0.69$ MPa

[1] In later versions there may be different parameters for different sets.

[2] The cohesion is dependent on the friction angle. The friction angle given in °.

2.3   In situ stresses

Two different stress domains were defined in Simpevarp /Hakami and Min 2005/. The state of stress was estimated for each domain as a function of depth and these estimations were used to select the confining stress levels for the numerical loading tests representing the conditions at repository depth, 500 m. These values are given in Table 2-9. The stresses diverge in magnitude between the two different stress domains but their orientation is similar. For both lithological domains A and B only the stress domain I was considered for direct loading test to enable direct comparisons of rock mass properties.

Table 2-9. In situ stress magnitude and orientation for both stress domains at 500 m depth.

	Stress domain I			Stress domain II		
	$σ_1$	$σ_2$	$σ_3$	$σ_1$	$σ_2$	$σ_3$
Mean magnitude, MPa	32	14	9.5	16	9	5.5
Mean strike, °	132	90	42	132	90	42
Mean dip, °	0	90	0	0	90	0

3 Set-up of the model

3.1 Description of the numerical simulations

The parameters presented in Section 2.2.1 were used to generate the 3D fracture network used for extraction of fracture data into 3DEC.

The fracture networks were generated for two rock domains, RDA and RDB, based on the different fracture intensity in the two rock domains. Two different sets of parameters were used for P_{32} depending on the estimated relative proportion of sub-horizontal fractures in the rock mass.

For each rock domain 20 realisations of the same fracture network (i.e. with all input parameters equivalent) are simulated for the "base case" (i.e. 20% of sub-horizontal fractures in the rock mass).

Only open fractures (including partly open fractures) were generated in the DFN model. Based on the results of laboratory tests, the assumption that sealed fractures do not significantly influence the mechanical behaviour of the rock mass was made.

When the 3D fracture networks are generated 2D vertical sampling planes oriented parallel to the horizontal in situ stresses (σ_H and σ_h) are extracted. The trace data on these planes are used for input in 3DEC. The identification of each fracture set is maintained throughout the process allowing assigning different mechanical properties to the different fracture sets.

In Figure 3-1 an example of generated fracture traces in a vertical plain is shown. In Figure 3-2 the corresponding 3DEC model is shown, and in Figure 3-3 the contact points along each fracture in the 3DEC model are illustrated.
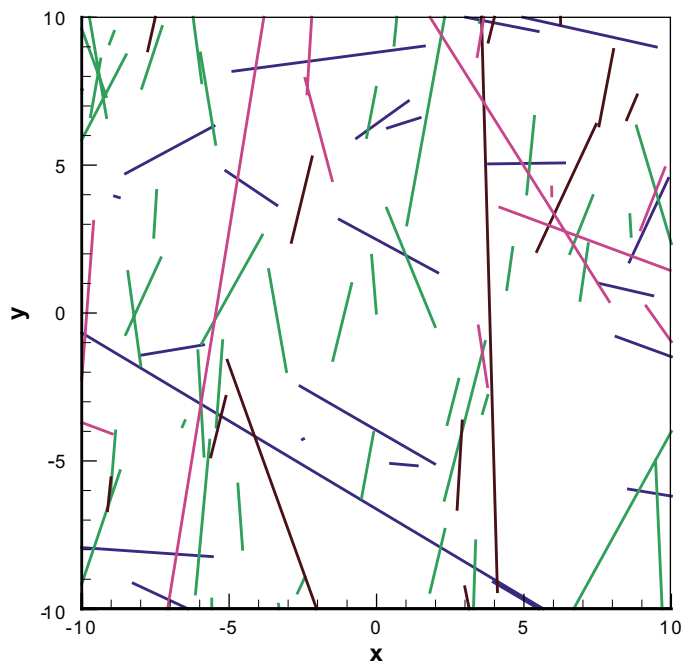
Figure 3-1. *Example of fracture traces in a vertical plan. Fracture traces from different fracture sets have different colours.*
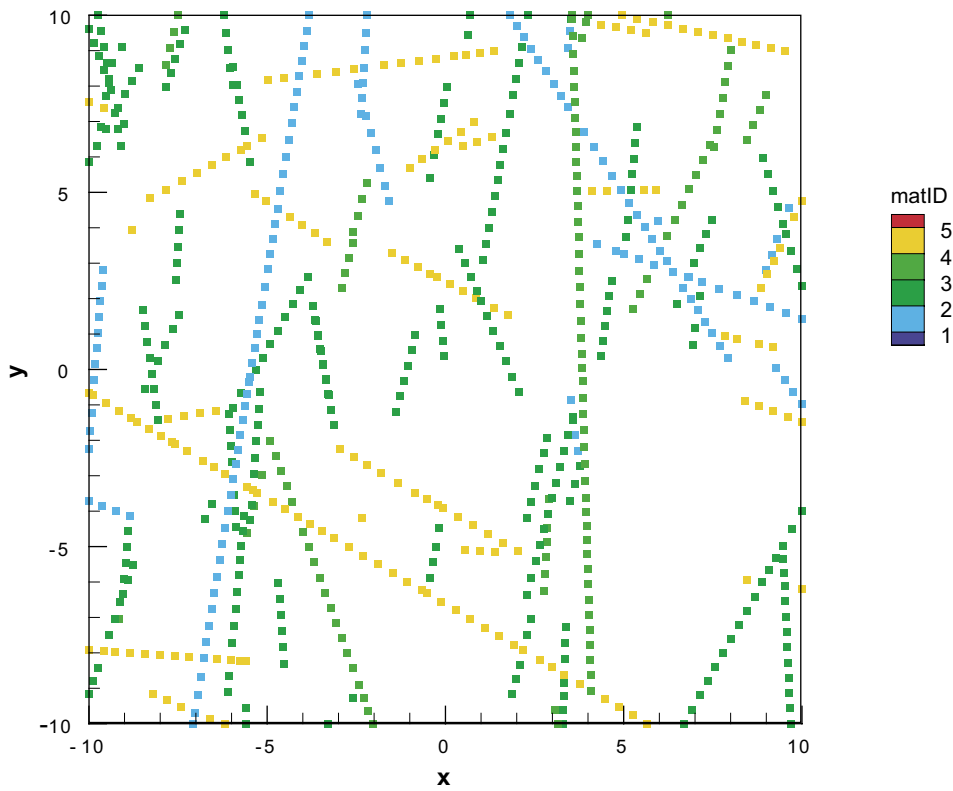
Figure 3-2. 3DEC model generated from the fracture traces shown in Figure 3-1.

Figure 3-3. Contact points along fractures in the 3DEC model.

The result in the form of vertical stress-vertical strain and horizontal strain–vertical strain curves from one simulation with 3DEC is shown in Figure 3-4.

The deformation modulus, E_m, and Poisson's ratio, v_m, of the rock mass are evaluated from stress-vertical strain and horizontal strain – vertical strain curves. The strength parameters of the rock mass, uniaxial strength, UCS_m, cohesion, c_m, and friction, φ_m, are evaluated from simulations with different confining stress. The following equations are used:

$$\phi_m = \arcsin(k-1/_{k+1}) \tag{3.1}$$

$$UCS_m = \sigma_{vfb} + k \cdot \sigma_b \tag{3.2}$$

$$c_m = UCS_m \cdot (1-\sin \phi_m)/_2 \cdot \cos\phi_m \tag{3.3}$$

where $k = \dfrac{(\sigma_{vfa} - \sigma_{vfb})}{(\sigma_a - \sigma_b)}$ and σ_{vfa}, σ_{vfb}, σ_a and σ_b are the principal vertical stresses at failure at two confining stress levels a and b.

Distributions of the four rock mass parameters (E_m, v_m, c_m, and φ_m) are estimated at a block scale of 20 m, using the software 3DEC for the rock mechanical modeling part and GoldSim for subsequent Monte-Carlo simulations.

The procedure is in more detail described in /Olofsson and Fredriksson 2005/.

The uncertainty of a model can be separated into conceptual uncertainty, data uncertainty and spatial variability. The conceptual uncertainty originates from an incomplete understanding of the principal structure of the analyzed system and its interacting processes. This uncertainty is not further discussed.

Data uncertainty concerns the uncertainty in parameter values being used in a model; it may be caused by measuring errors, interpretation errors or uncertainty in extrapolation of spatially variable parameters.
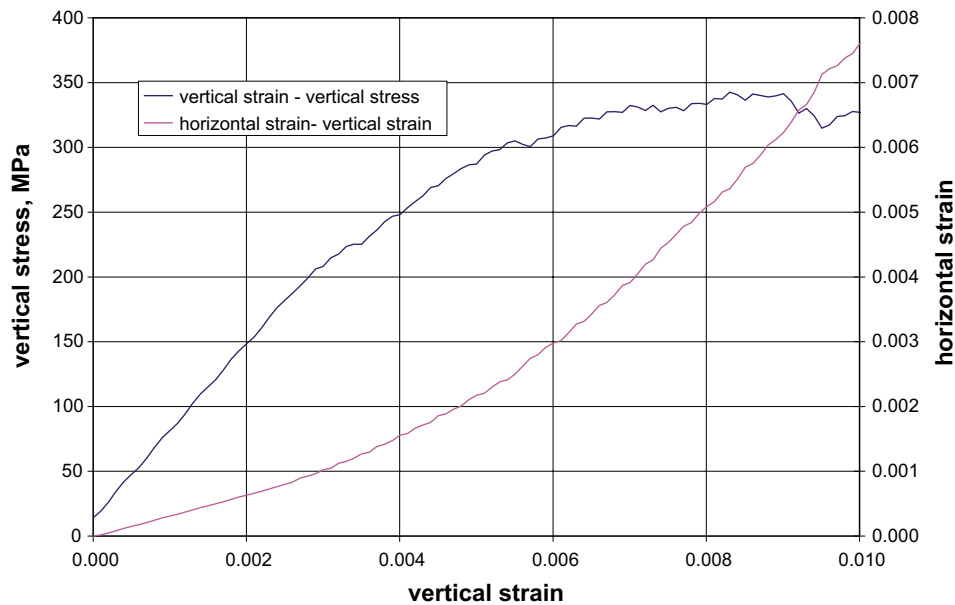
Figure 3-4. *Example of stress- strain curves.*

Spatial variability concerns the variation in space of a parameter value; although this is not strictly an uncertainty, in combination with practical limitations in rock characterization, it constitutes an indirect source for data uncertainty. Hence, in the following, no distinction is made to what extent the estimated rock mass parameter distributions relate to spatial variability and/or data uncertainty.

In the case of the present data, stochastic material properties of intact rock and of fractures are approximated by empirical, truncated, normal distributions that are defined by their mean, standard deviation, minimum and maximum values (Table 3-1). Likewise, the DFN geometry is given as stochastic distributions.

Ideally, rock mass property distributions could be estimated by iterative 3DEC simulations involving numerous stochastic DFN realizations, where the DFN geometry and material property parameters are allowed to take on any value from their defined input distributions. However, such a direct approach becomes impractical due to its computational demand and limitations in parameter descriptions in 3DEC.

Instead, a simpler stochastic approach is used. Here, 3DEC is only used to estimate the DFN geometry-induced variability and the influence input material parameters (intact rock and fractures) have on rock mass properties. The combined effect of DFN geometry-induced variability and the material property-induced variability is estimated by Monte-Carlo simulations using a simple GoldSim model.

The procedure for management of uncertainty is described in the methodology report /Olofsson and Fredriksson 2005/.

3.2   Assumptions

The key concept used here is that the rock mass variability depending on the geometry of the fracture network (DFN-model) can bee evaluated independent of the variability from the variation of mechanical properties of the fractures and the intact rock i.e they are independent of another. The variability can be evaluated separately and the total variability can be estimated by superimposing the effects of the two components.

Sealed fractures are not explicitly simulated and test samples containing sealed fractures are treated as "intact rock" samples.

3.3   Indata to the numerical simulations

From the laboratory we have uniaxial and tiaxial load tests. For each rock type more uniaxial load test are performed than triaxial tests. Therefore the uniaxial tests give a better basis to estimate the variation in strength, UCS_i and type of distribution than the triaxial tests. From the triaxial tests it is possible to estimate of the variation of the friction angle, φ_i of the intact rock. The relationship between, φ_i, c_i and UCS_i is

$$UCS_i = \frac{2 \cdot c_i \cdot \cos \phi_i}{1 - \sin \phi_i} \tag{3.4}$$

Knowing the distribution of the uniaxial strength, UCS_i, and the distribution of the friction angle, φ_i, the distribution of the cohesion, c_i, (Equation 3.4) can be determined by Goldsim simulations, assuming that the cohesion, c_i, and the friction angle, φ_i, are not correlated.

However to test whether the assumption of uncorrelated c_i and φ_i is actually reasonable, triaxial test data were simulated from a first estimate of the distributions of c_i and φ_i. These "simulated triaxial test data" were then compared to the "real triaxial test data" (Figure 3-5a and b). As can be seen, the given c_i and φ_i produce a too narrow range for RDA and a too wide range for RDB, if comparing simulated and measured UCS_i-values. Also, the given lower limit of UCS_i for RDB is higher than the real data indicates. To conclude, the given input parameters define an over-determined system.

In order to adjust c_i and φ_i, so as to better match the tri- and uniaxial measured data, c_i is instead calculated from UCS_i and φ_i (which also are assumed uncorrelated), using (Equation 3.5). The UCS_i limits of RDB are redefined according to uniaxial loading test measurements. As can be seen in Figure 3-6a and b, the new "simulated triaxial tests" match the real data better.

$$c_r = \frac{UCS\left(1 - \sin\phi_r\right)}{2\cos\phi_r}$$
(3.5)
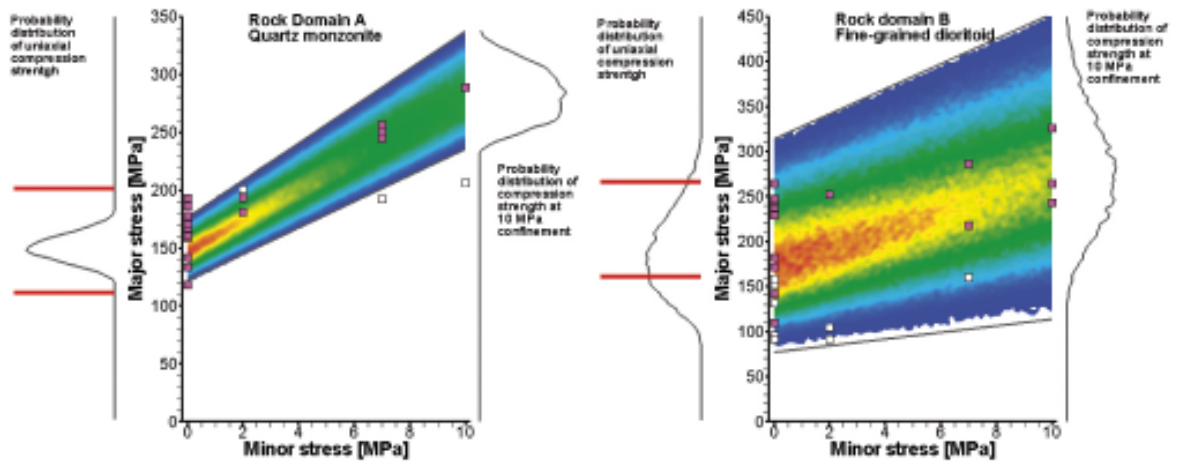
Figure 3-5a and b. *Probability distributions of simulated triaxial test data from given distributions of c_r and φ_r (assumed non-correlated). Pink boxes are real intact rock data and white boxes refer to sampled including sealed fractures. Red lines indicate given limits of UCS.*
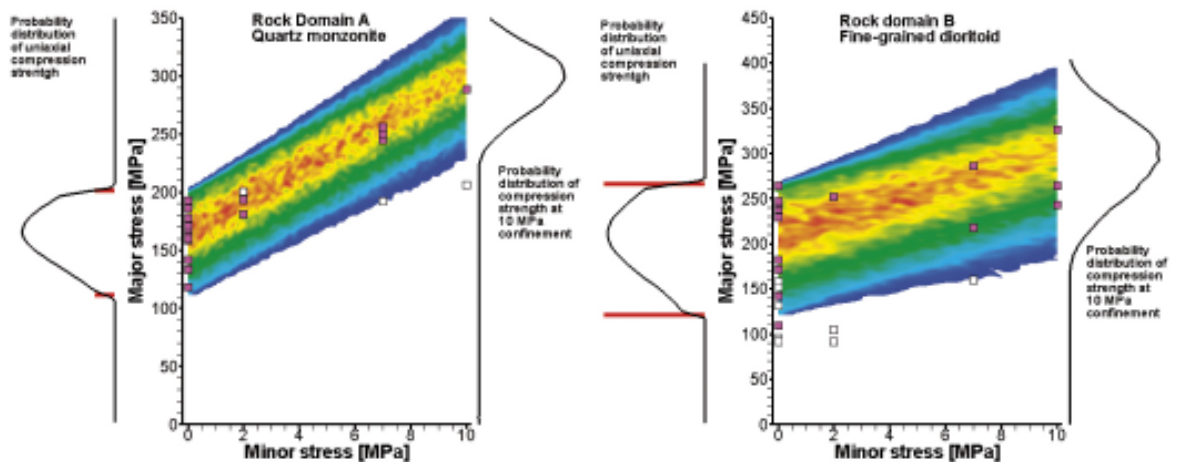
Figure 3-6a and b. *Probability distributions of simulated triaxial test data from given distributions of UCS_i and φ_i (assumed non-correlated). Pink boxes are real intact rock data and white boxes refer to sampled including sealed fractures. Red lines indicate modified limits of UCS_i.*

The new calculated c_i distributions are summarized in Table 3-1. As a consequence, c_i and φ_i become correlated and the correlation coefficient is –0.327 for RDA and –0.241 for RDB. As will be discussed later, the rock mass UCS of RDB depends strongly on c_i, and its large span (14–59), which is a direct consequence of the large range of φ_i, is found unrealistic. Instead, φ_i in (Equation 3.5) is always chosen such that the previous truncation limits of c_i (20–42) still apply for RDB. The increased range for c_i in RDA has a minor impact on rock mass UCS.

Statistical distributions of input parameters are shown in Table 3-2. The fracture properties are assumed to be equal for both rock domains. The cohesion and friction angles for intact rock of both domains, c_i and φ_i, are assumed to be independent (non-correlated). Statistics of the uniaxial tensile strengths, T_i, are also given.

Table 3-1. Cohesion for intact rock.

		Mean	Standard deviation	Min	Max
RDA	c_i (MPa)	22	3.2	14	29
RDB	$c_i^{(1)}$ (MPa)	32.5	5.4	(14)	(59)
	$c_i^{(2)}$ (MPa)	32.5	5.4	20	42

(1) Strictly applying (Equation 3.2).

(2) Applying the truncation limits of c_i (20–42).

Table 3-2. Input parameter and distributions for intact rock and fracture properties.

		Mean	Standard deviation	Min	Max
Intact rock, RDA	E_i (GPa)	80	10	70	90
	v_i (–)	0.27	0.05	0.18	0.33
	φ_i (°)	60	3	57	62
	c_i (MPa)	22	3.2	14	29
	T_i (MPa)	17	4	12	24
Intact rock, RDB	E_i (GPa)	85	10	70	110
	v_i (–)	0.26	0.03	0.19	0.31
	φ_i (°)	55	6	35	60
	c_i (MPa)	32.5	5.4	20	42
	T_i (MPa)	20	2	14	24
Fractures	K_n (MPa/mm)	100	32	49	179
	K_s (MPa/mm)	29	11	10	49
	φ_f (°)	32	4	24	40
	c_f (MPa)	$2.35-0.058\times\varphi_f$	0.25	$c_{f\,mean}-0.37$	$c_{f\,mean}+0.69$

4 Simulations

4.1 Description of the procedure

The distributions of rock mass properties being estimated here (E_m, ν_m, c_m, and φ_m) are assumed to consist of two main components: a) an intrinsic variability component caused by its stochastic DFN geometry and b) a component induced by stochastic material properties of fractures (K_n, K_s, φ_f, and c_f) and those of intact rock (E_i, ν_i, φ_i, c_i, and T_i). Further, these two components are assumed to be independent, such that the total rock mass property distributions can be estimated by superimposing the DFN geometry-based and the material property-related variability components. The procedure outline can be summarized as follows:

1. The variability component caused by stochastic fracture network geometry is evaluated for multiple DFN realizations; these are all assigned mean material-property values.

2. The influence that each individual material property has on the rock mass properties is estimated for one specific "average" realization; it is done by examining the effect on rock mass parameters as each material property is assigned its minimum and maximum parameter values, while all other material properties are set to their mean values.

3. Next, the effect that variable material properties have on the rock mass is then estimated in a stochastic framework; material parameters are sampled from their empirical distributions (Table 3-1) and applied to the relationships obtained in step 2, to provide estimates of their impact on rock mass property variability.

4. Finally, the DFN geometry-induced and the material property-related components are superimposed to estimate the total ranges of rock mass parameter distributions.

4.2 DFN geometry-induced rock mass variability

4.2.1 Simulations parallel to σ_H, Rock Domain A

The first variability component, relating to variability arising from the stochastic fracture net work geometry alone, is evaluated by 3DEC modeling of DFN realizations with fracture traces in a plane parallel to σ_1 subject to two confining stresses: 32 MPa and 8 MPa (see Section 2.3). 32 MPa is equivalent to σ_1 in stress domain I, and 8 MPa is selected as 25% of this value. The mean material property values (Table 3-2) are assigned both to fractures and to the intact rock. Out of 20 generated DFN-realizations 3DEC could generate zone division for 17 of them, 3 realizations had to be rejected.

The numerical models were loaded with a constant velocity in the vertical direction while the horizontal confining stress, σ_a respective σ_b, was kept constant during the loading test. The deformation modulus, E, Poisson's ratio, ν, and the vertical stress at failure, σ_{vf}, were evaluated at both confining stress levels to provide an estimation of φ_m and c_m.

The evaluated rock mass parameters at confing stress 32 MPa and 8 MPa are presented in Appendix A. In Figure 4-1, Figure 4-2, Figure 4-3 and Figure 4-4 the distributions for deformation modulus and Poisson's ratio are illustrated.
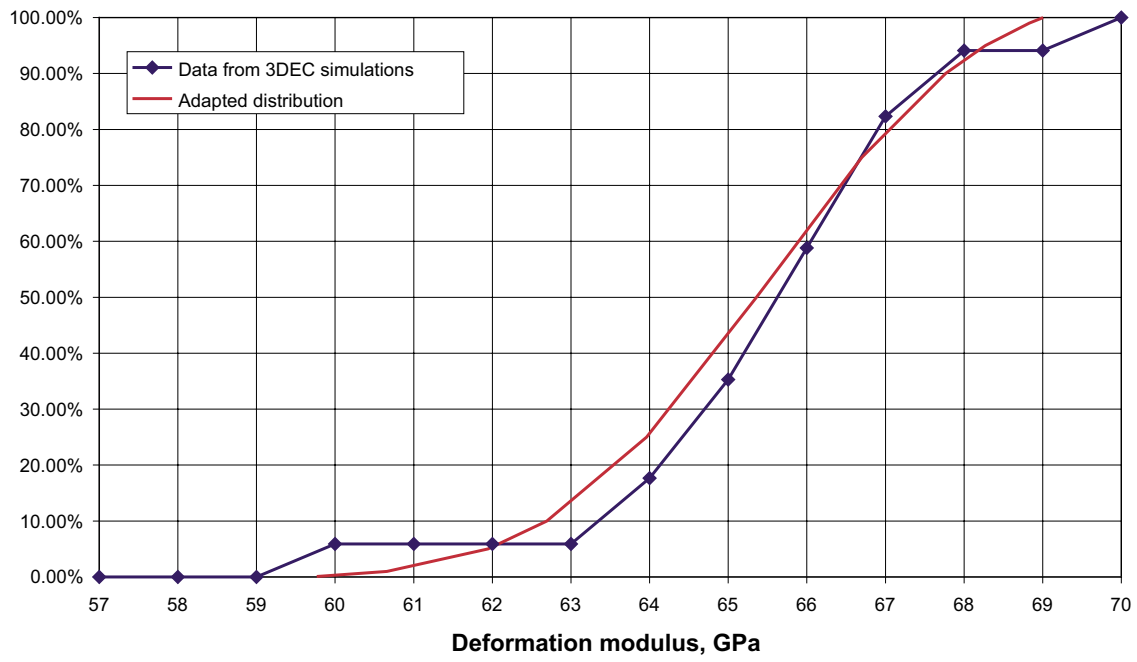
Figure 4-1. *Distribution of deformation modulus at high confining stress level (32.0 MPa), Rock Domain A, trace plane parallel to σ_H.*
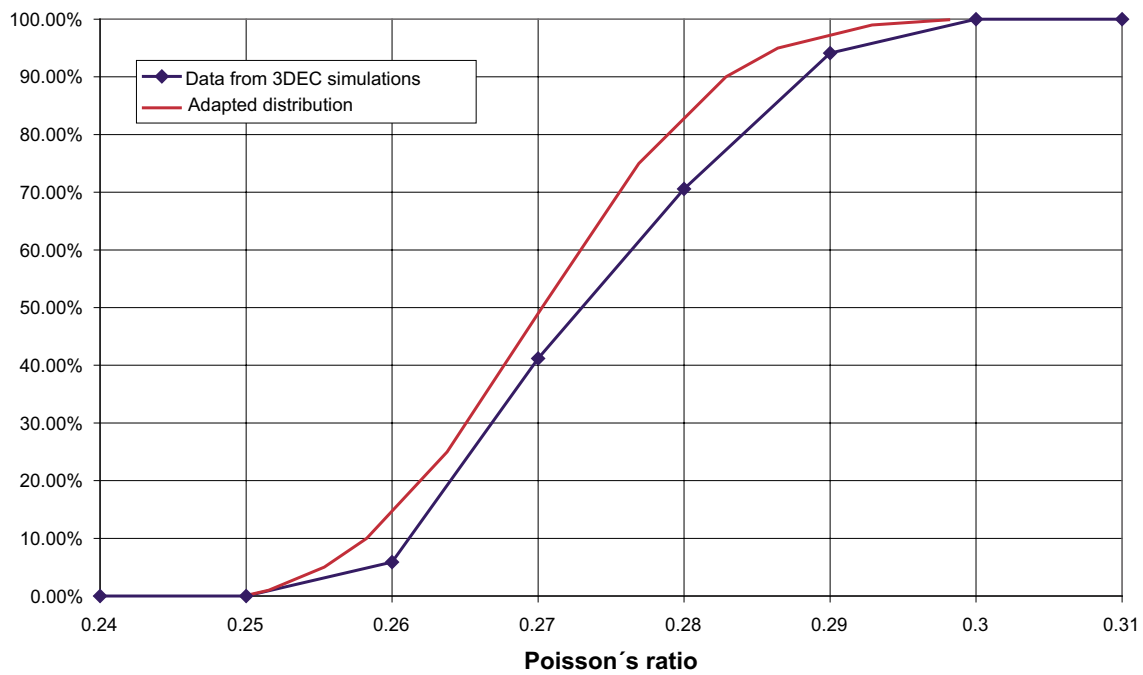
Figure 4-2. *Distribution of Poisson's ratio at high confining stress level, (32 MPa) Rock Domain A, trace plane parallel to σ_H.*
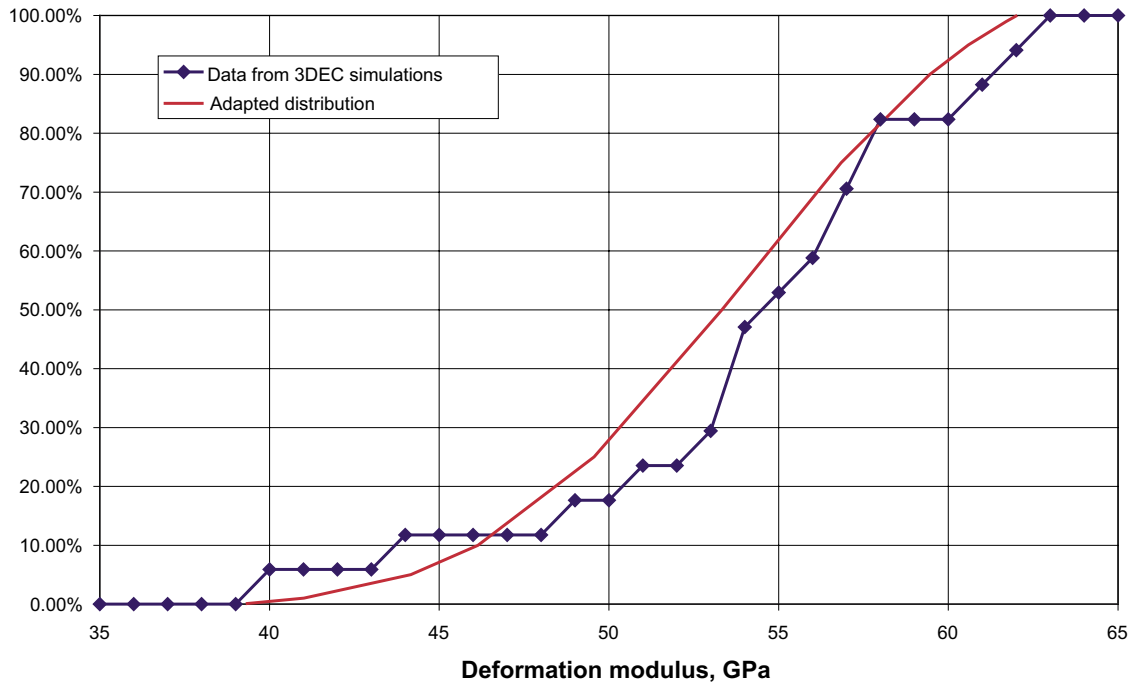
Figure 4-3. *Distribution of Deformation modulus at low confining stress level, (8.0 MPa) Rock Domain A, trace plane parallel to σ_H.*
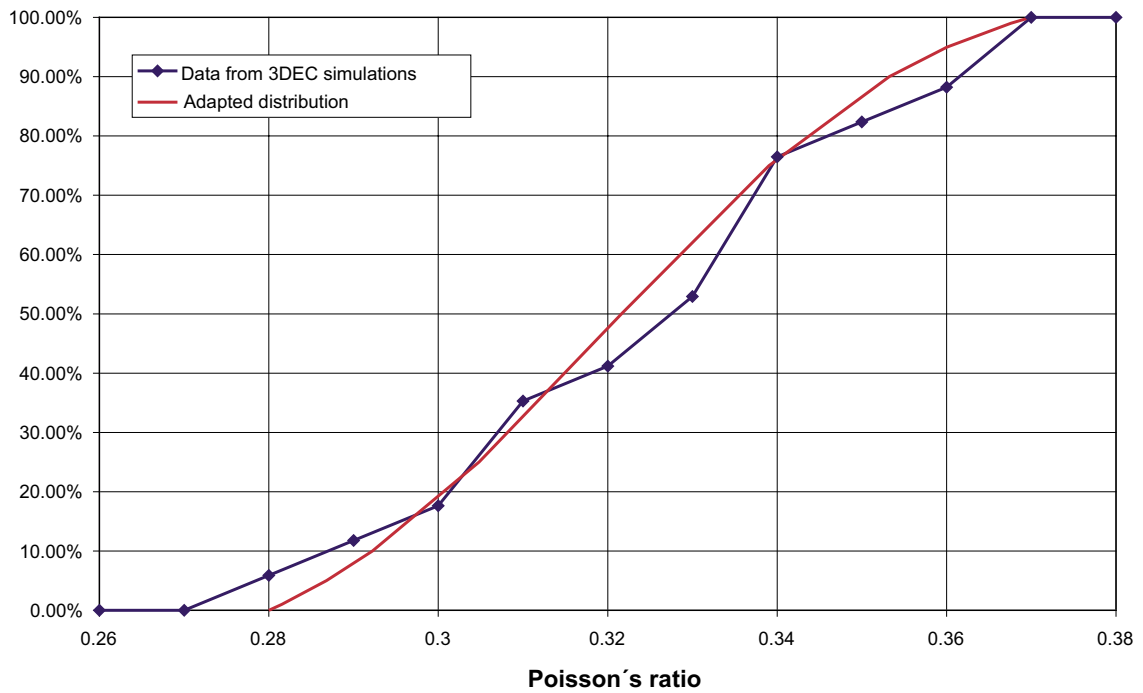
Figure 4-4. *Distribution of Poisson's ratio at low confining stress level, (8,0 MPa) Rock Domain A, trace plane parallel to σ_H.*

The evaluated cohesion and friction angle of the rock mass for each simulation are presented in Appendix A. These parameters were evaluated by fitting a straight line between the vertical stress at failure at both stress levels. The uniaxial compressive strength of the rock mass has been calculated from the evaluated cohesion and friction angle. The distributions of friction angle, cohesion and uniaxial compressive strength are shown in Figure 4-5, Figure 4-6 and Figure 4-7.
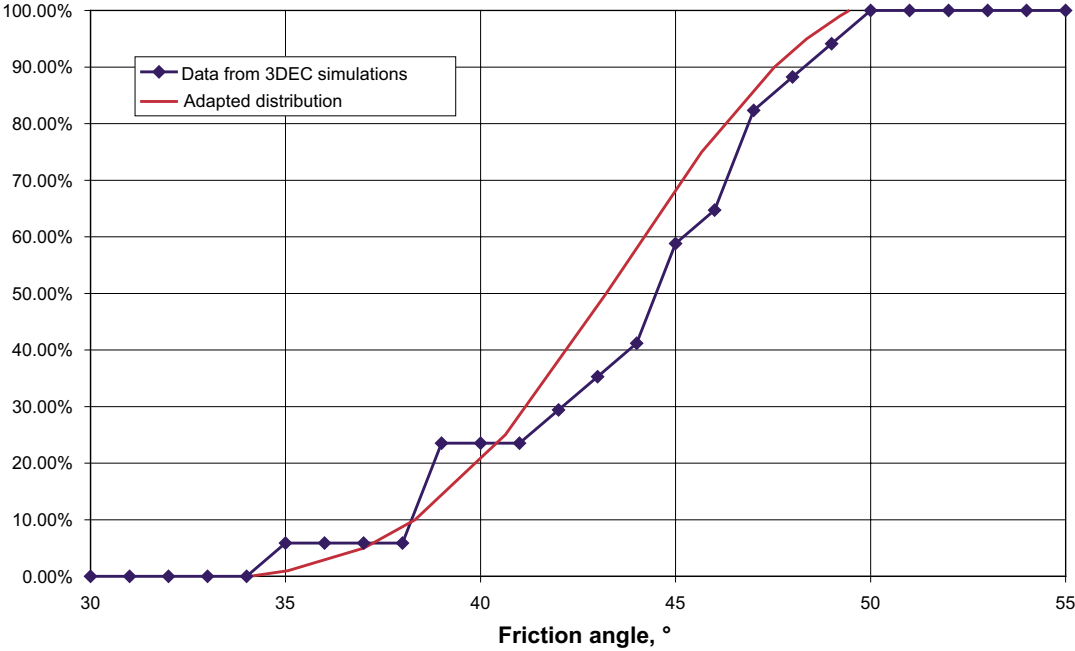
Figure 4-5. *Distribution of friction angle, rock mass in Rock Domain A, trace plane parallel to σ_H.*
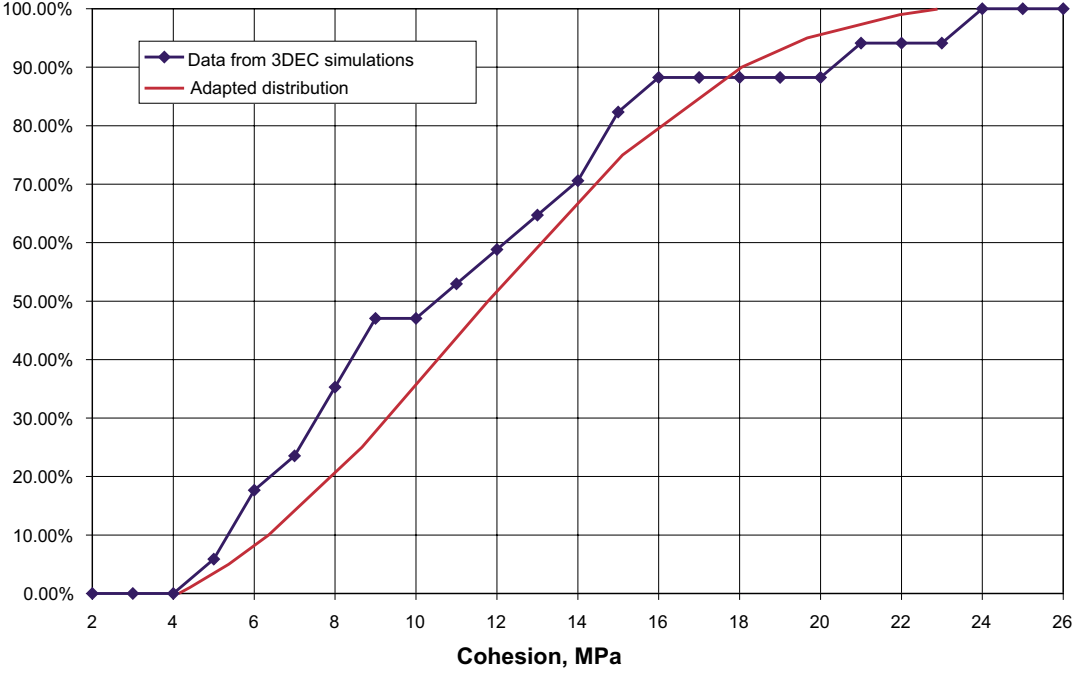
Figure 4-6. *Distribution of cohesion, rock mass in Rock Domain A, trace plane parallel to σ_H.*
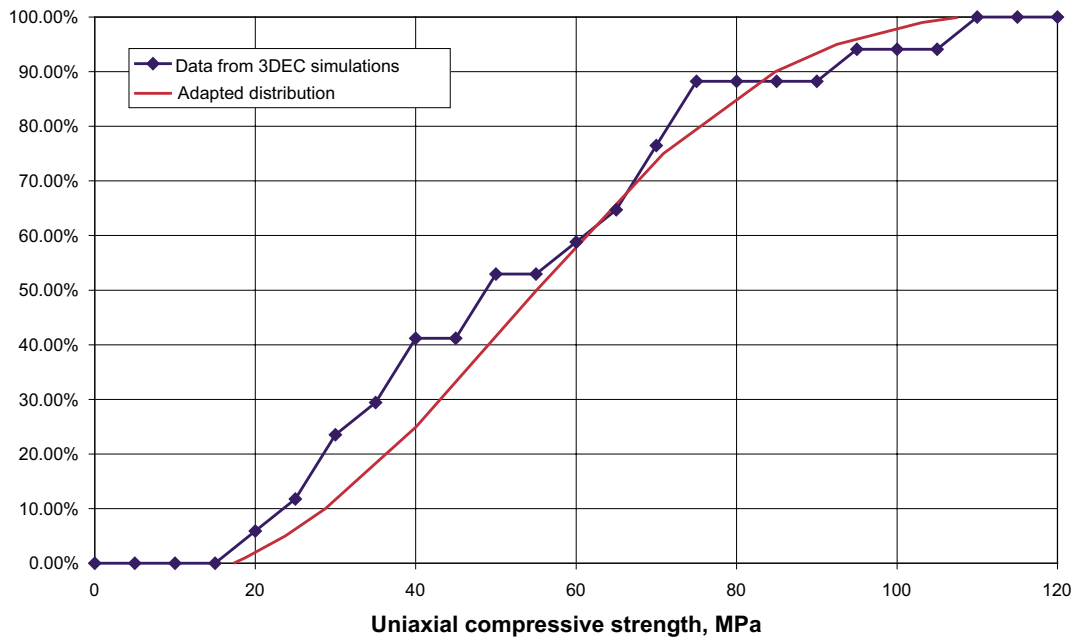
Figure 4-7. *Distribution of the uniaxial strength of the rock mass in Rock Domain A, trace plane parallel to σ_H.*

Some realizations give a very low value for the uniaxial strength of the rock mass. If you examine these realizations in detail you see that usually at least one fracture cuts of a corner of the block and sliding occurs along this fracture. One example is illustrated in Figure 4-8, where one fracture cut of the lower right corner of the model. The results of these realizations are omitted when the final distributions for φ_m and c_m are calculated. The final obtained distributions of $E_{m\ 32\ MPa}$, $v_{m\ 32\ MPa}$, $E_{m\ 8\ MPa}$, $v_{m\ 8\ MPa}$, φ_m and c_m are summarized in Table 4-1 for rock domain A. The distributions of parameters that are given in this table only account for the influence of variation in the fracture pattern on the rock mass properties (as input mechanical parameters are constant).
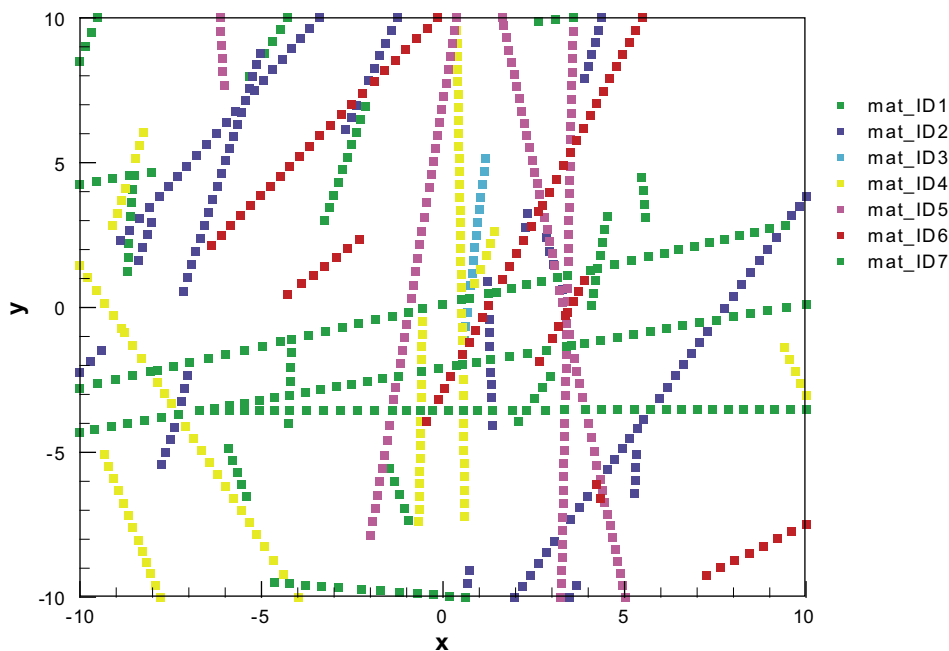
Figure 4-8. *Fracture traces for realisation nr 8. mat_IDi refers to the fracture sets.*

Table 4-1. DFN geometry-induced variability in rock mass properties of Rock Domain A, parallel to σ_1.

	Mean	Standard deviation	Min	Max
$E_{m\ 32\ MPa}$ (GPa)	65.5	2.2	59.6	69
$v_{m\ 32\ MPa}$ (−)	0.27	0.01	0.25	0.3
$E_{m\ 8\ MPa}$ (GPa)	54	6	39.1	62
$v_{m\ 8\ MPa}$ (−)	0.32	0.03	0.28	0.37
φ_m (°)	44.83	3.45	38.26	49.46
c_m (MPa)	$41.30 - 0.5954 \times \varphi_m$	3.96	$c_{m\ mean} - 5.58$	$c_{m\ mean} + 7.8$

4.2.2 Simulations parallel to σ_h, Rock Domain A

DFN realizations parallel to σ_h were also generated and loaded in 3DEC for two confining pressures: 14 MPa and 3.5 MPa (see Section 2.3). 14 MPa is equivalent to σ_2 in stress domain I, and 3.5 MPa is 25% of this value[1]. The mean material property values (Table 3-2) are assigned both to fractures and to the intact rock. Out of 20 generated DFN-realizations 3DEC could generate zone division for 19 of them, 1 realization had to be rejected. The evaluated rock mass parameters are presented in Appendix B.

The evaluated rock mass parameters and distributions at 14 MPa are presented in Figure 4-9 and Figure 4-10, and the parameters and distributions evaluated at 3.5 MPa in Figure 4-11 and Figure 4-12. The cohesion and friction angle of the rock mass and the distributions are presented in Figure 4-13 and Figure 4-14. These parameters were evaluated by fitting a straight line between the vertical stress at failure at both stress levels. The uniaxial compressive strength of the rock mass has been calculated from the evaluated cohesion and friction angle, see Figure 4-15.
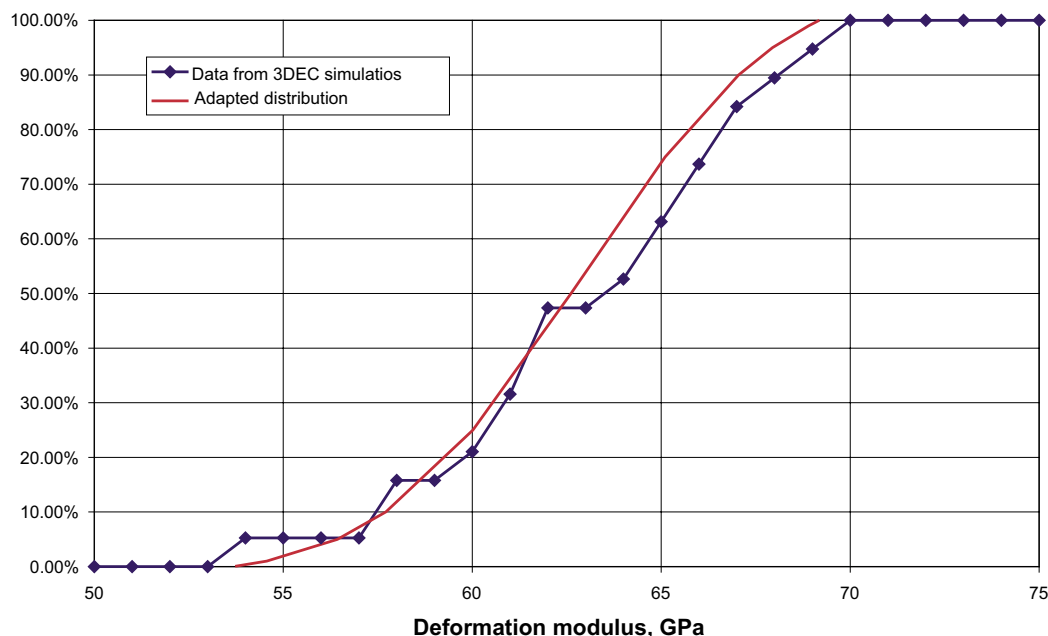
Figure 4-9. *Distribution of deformation modulus at high stress level (14.0 MPa), Rock Domain A, trace plane parallel to σ_h.*

---

[1] According to the stress model presented in Section 2.3 the minimum horizontal stress σ_h in Simpevarp corresponds to σ_3. However the modelling on the vertical trace planes extracted parallel to σ_h were loaded at confining stresses corresponding to σ_2 in-situ stresses.
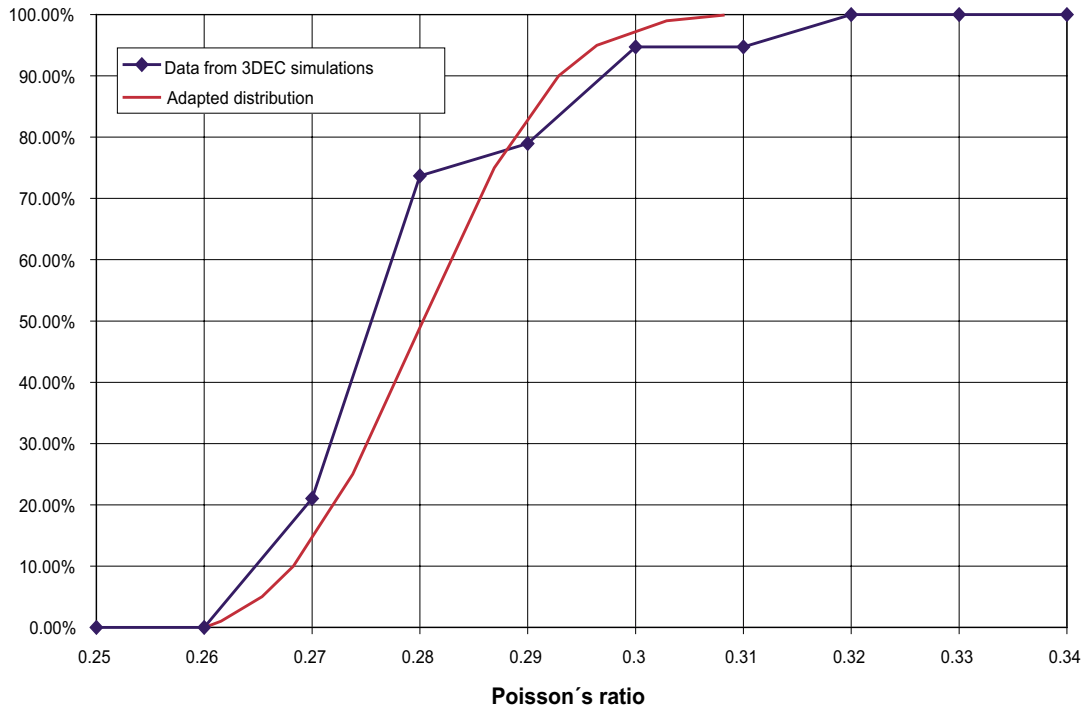
Figure 4-10. *Distribution of Poisson's ratio at high stress level, (14.0 MPa) Rock Domain A, trace plane parallel to σ_h.*
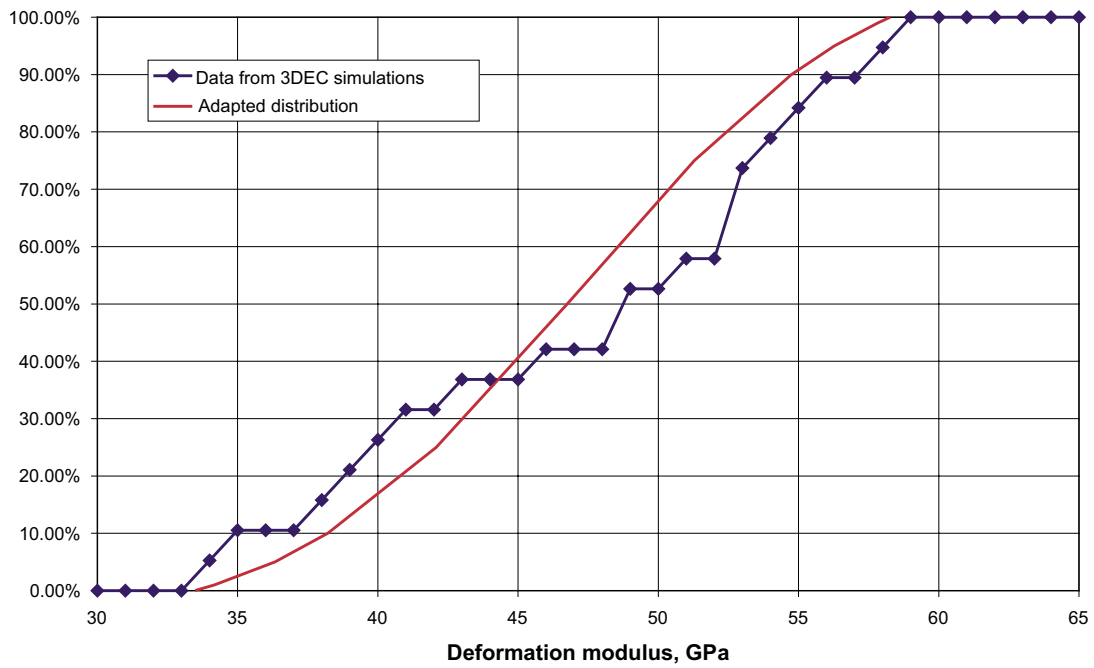
Figure 4-11. *Distribution of deformation modulus at low stress level (3.5 MPa), Rock Domain A, trace plane parallel to σ_h.*
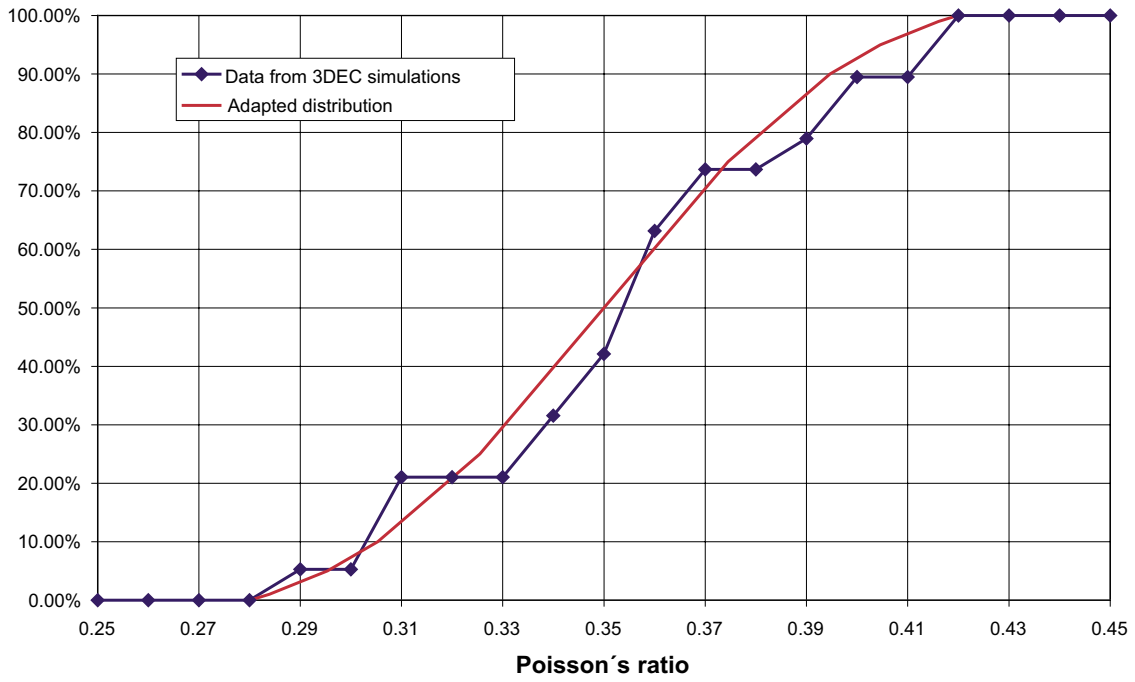
Figure 4-12. *Distribution of Poisson's ratio at low stress level, (3.5 MPa) Rock Domain A, trace plane parallel to σ_h.*
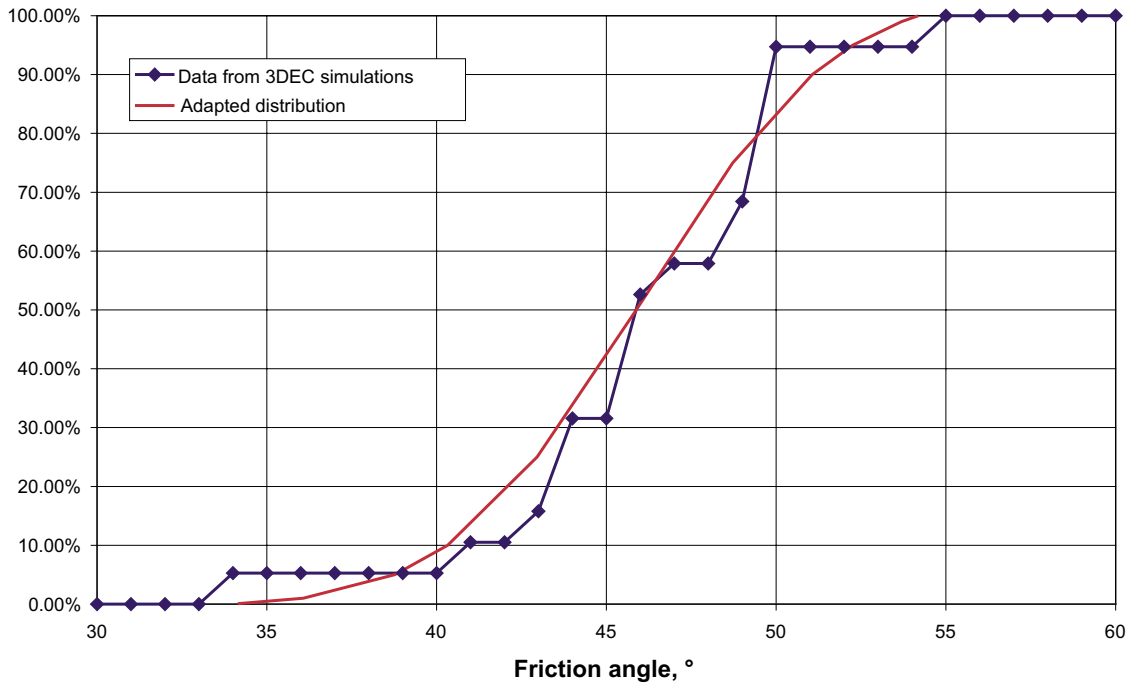
Figure 4-13. *Distribution of friction angle, rock mass in Rock Domain A, trace plane parallel to σ_h.*
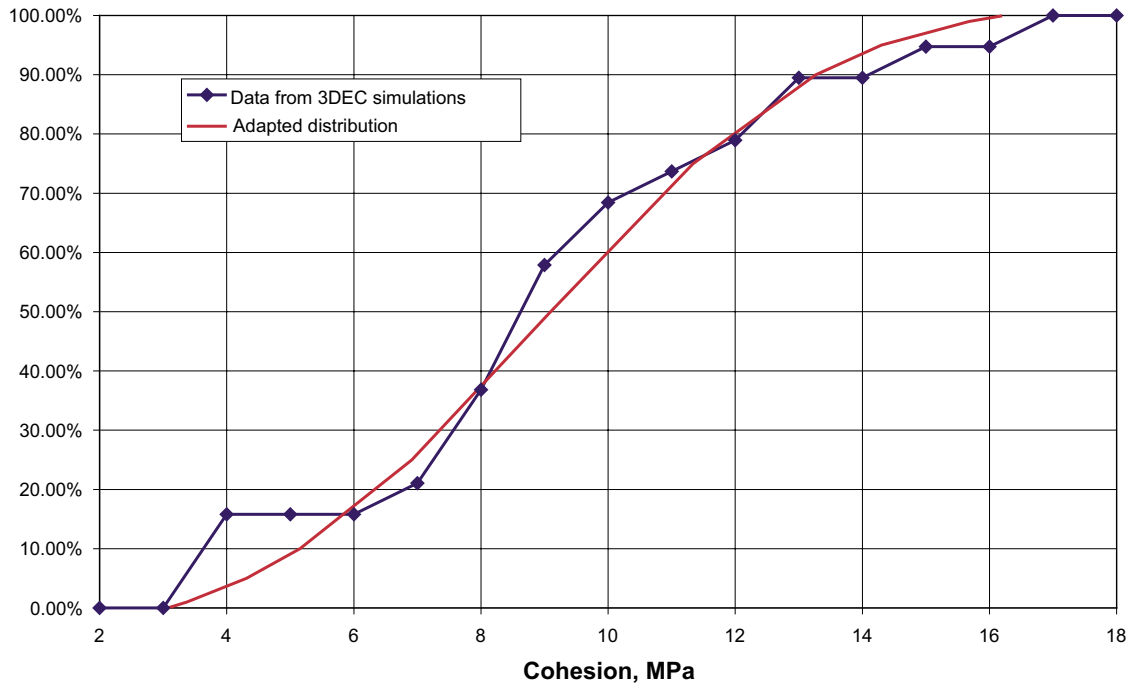
Figure 4-14. *Distribution of cohesion, rock mass in Rock Domain A, trace plane parallel to σ$_h$.*
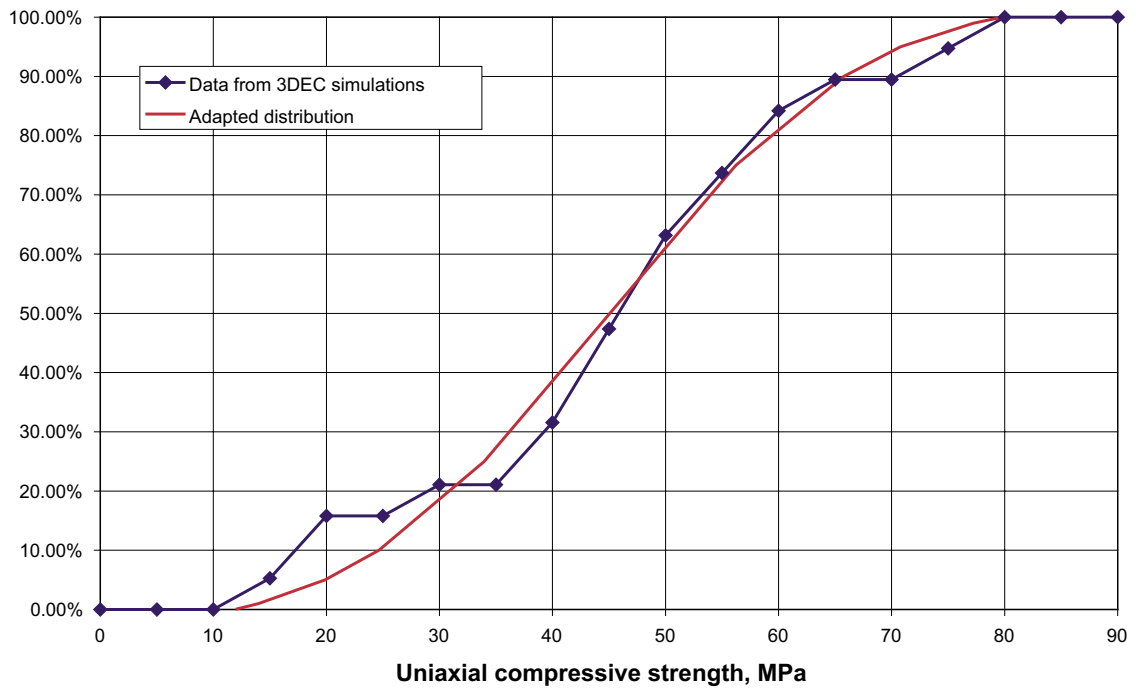
Figure 4-15. *Distribution of the uniaxial strength of the rock mass in Rock Domain A, trace plane parallel to σ$_h$.*

Table 4-2. DFN geometry-induced variability in rock mass properties of Rock Domain A, parallel to σ_2.

	Mean	Standard deviation	Min	Max
$E_{m\ 14\ MPa}$ (GPa)	62.9	4.1	53.6	69.2
$\nu_{m\ 14\ MPa}$ (−)	0.28	0.01	0.26	0.31
$E_{m\ 3.5\ MPa}$ (GPa)	47.1	7.9	33.5	58.3
$\nu_{m\ 3.5\ MPa}$ (−)	0.35	0.04	0.28	0.42
φ_m (°)	46	4.4	33.7	54.2
c_m (MPa)	9	3.6	3.1	16.2

The final obtained distributions of $E_{m\ 14\ MPa}$, $\nu_{m\ 14\ MPa}$, $E_{m\ 3.5\ MPa}$, $\nu_{m\ 3.5\ MPa}$, φ_m and c_m are summarized in Table 4-2 for rock domain A.

4.2.3   Simulations parallel to σ_H, Rock Domain B

DFN realizations parallel to σ_H were also generated for Rock Domain B and loaded in 3DEC for two confining pressures: 32 MPa and 8 MPa (see Section 2.3). 32 MPa is equivalent to σ_1 in stress domain I, and 8 MPa is 25% of this value. The mean material property values (Table 3-2) are assigned both to fractures and to the intact rock. Out of 20 generated DFN-realizations 3DEC could generate zone division for 19 of them, 1 realization had to be rejected. The evaluated rock mass parameters for each realization are presented in Appendix C.

The evaluated rock mass parameters at 32 MPa are presented in Figure 4-16 and Figure 4-17, and the parameters evaluated at 8 MPa in Figure 4-18 and Figure 4-19. The cohesion and friction angle of the rock mass are presented in Figure 4-20 and Figure 4-21. These parameters were evaluated by fitting a straight line between the vertical stress at failure at both stress levels. The uniaxial compressive strength of the rock mass has been calculated from the evaluated cohesion and friction angle, see Figure 4-22.
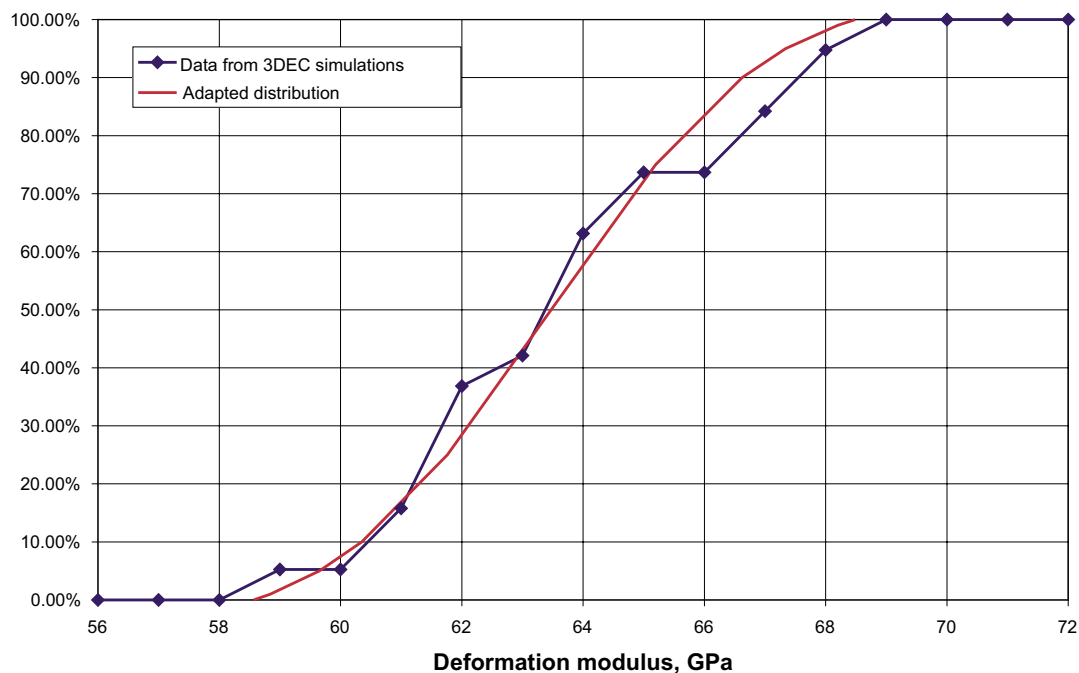
Figure 4-16. *Distribution of deformation modulus at high stress level (32.0 MPa), Rock Domain B, trace plane parallel to σ_H.*
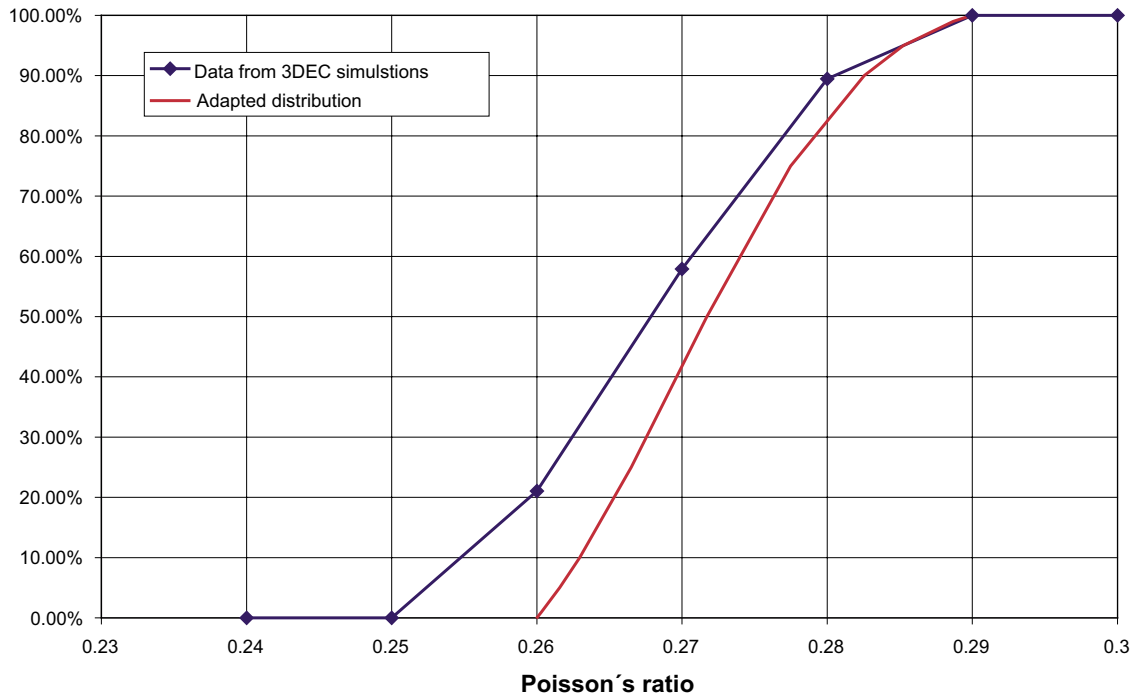
Figure 4-17. *Distribution of Poisson's ratio at high stress level (32.0 MPa), rock Domain B, trace plane parallel to* σ_H.
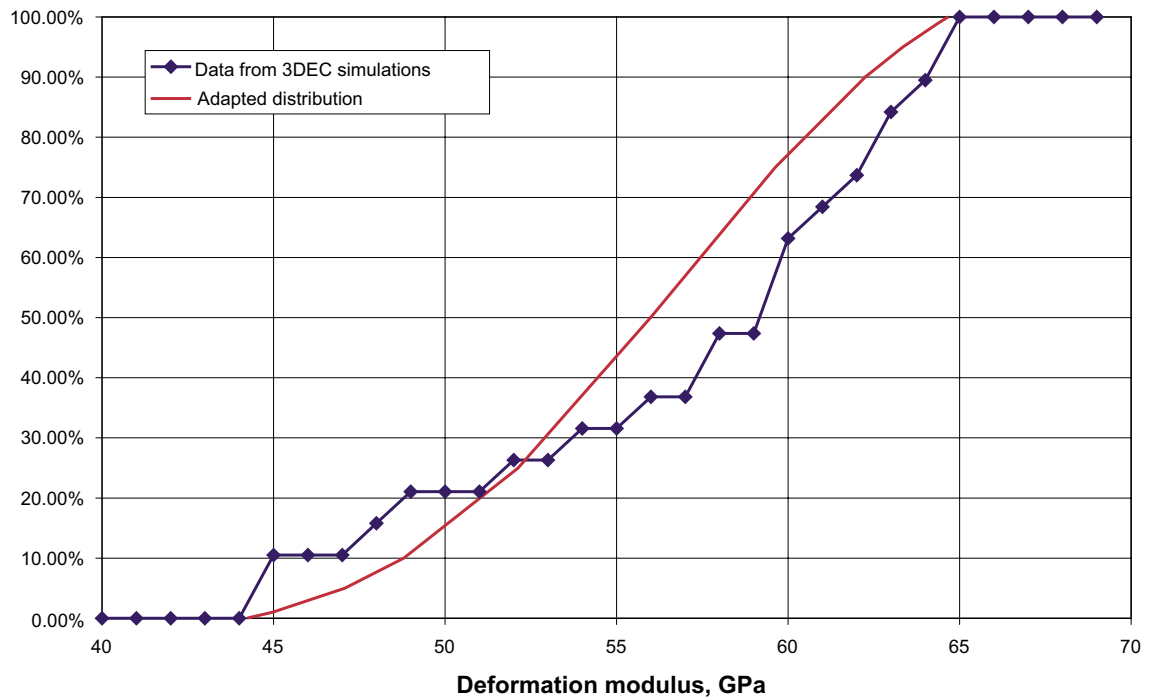
Figure 4-18. *Distribution of deformation modulus at low stress level (8.0 MPa), Rock Domain B, trace plane parallel to* σ_H.
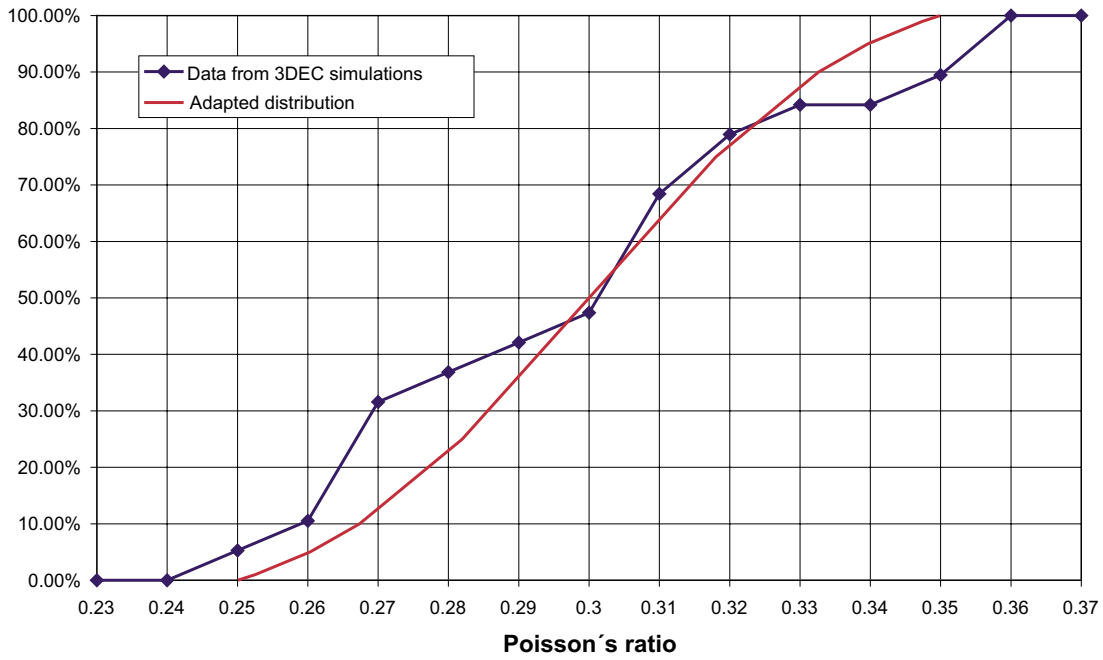
Figure 4-19. *Distribution of Poisson's ratio at low stress level, (8.0 MPa) Rock Domain B, trace plane parallel to σ_H.*
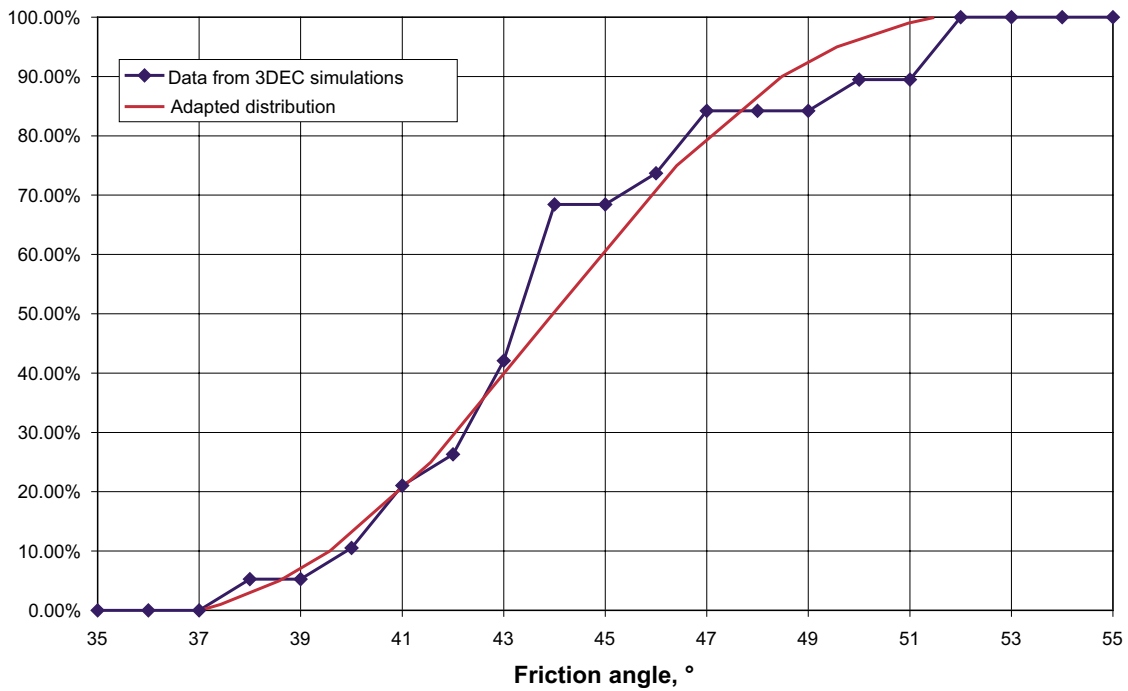
Figure 4-20. *Distribution of friction angle, rock mass in Rock Domain B, trace plane parallel to σ_H.*
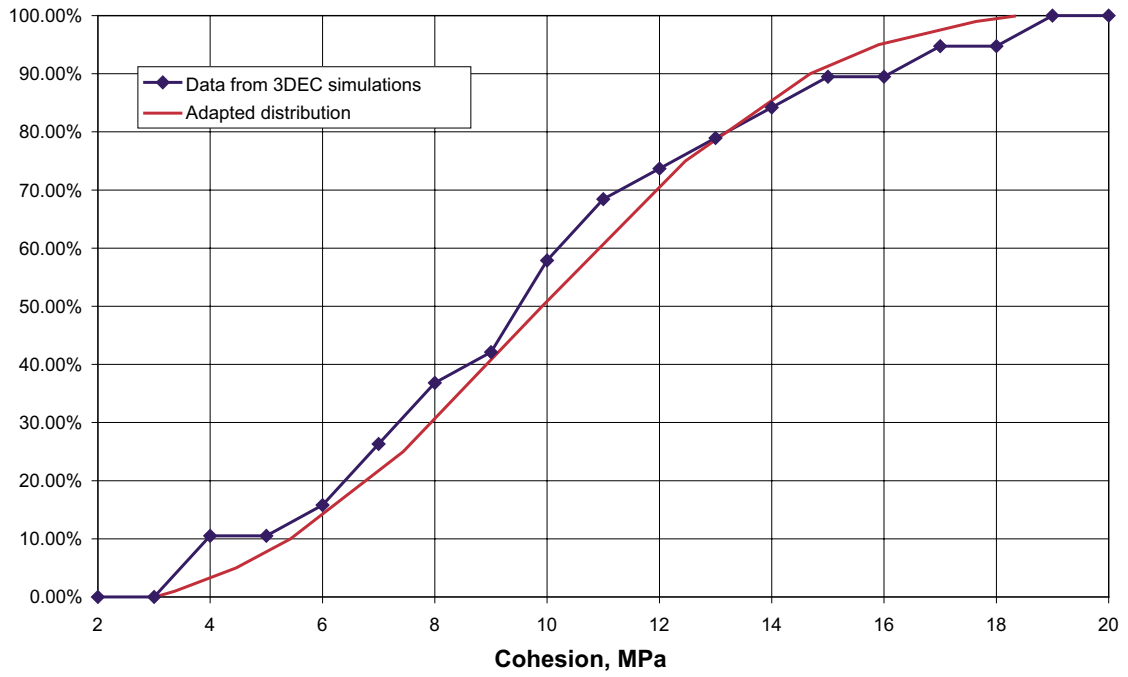
Figure 4-21. *Distribution of cohesion, rock mass in Rock Domain B, trace plane parallel to σ_H.*
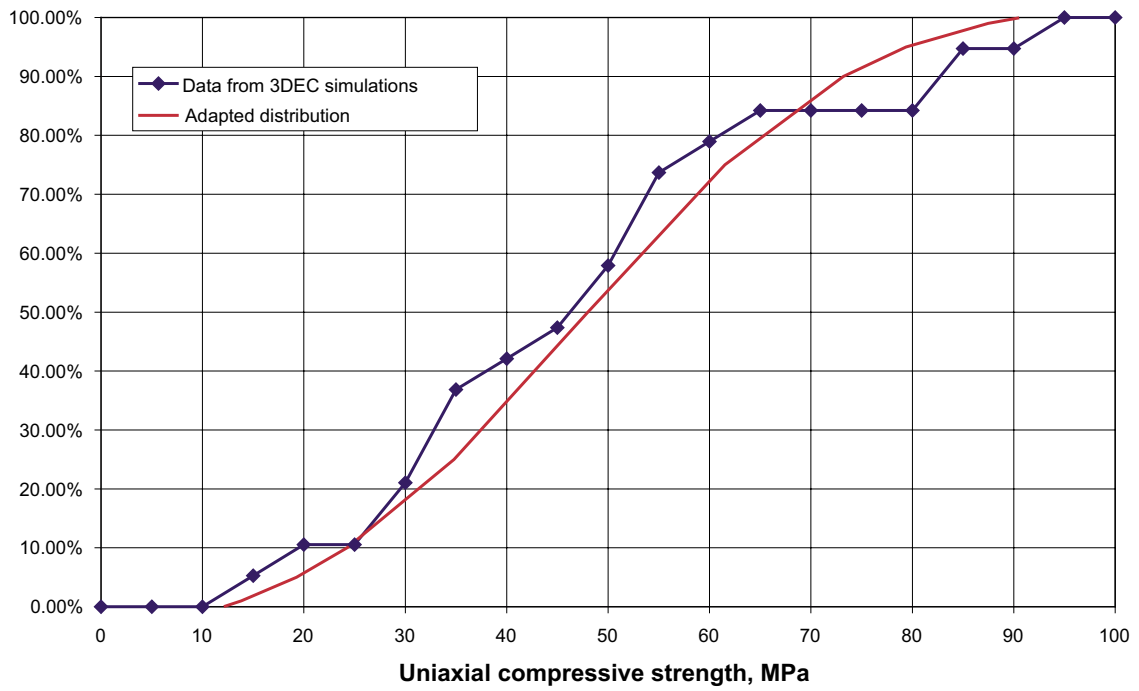
Figure 4-22. *Distribution of the uniaxial strength of the rock mass in Rock Domain B, trace plane parallel to σ_H.*

Table 4-3. DFN geometry-induced variability in rock mass properties of Rock Domain B.

	Mean	Standard deviation	Min	Max
$E_{m\ 32\ MPa}$ (GPa)	63.46	2.78	58.56	68.50
$v_{m\ 32\ MPa}$ (−)	0.27	0.01	0.26	0.29
$E_{m\ 8\ MPa}$ (GPa)	56.67	6.54	44.19	64.67
$v_{m\ 8\ MPa}$ (−)	0.30	0.03	0.25	0.35
φ_m (°)	44.93	3.57	39.76	51.52
c_m (MPa)	$0.3349 \times \varphi_m - 4.16$	5.4	$c_{m\ mean} - 6.7$	$c_{m\ mean} + 11.7$

Some realizations give a very low value for the uniaxial strength of the rock mass. The same problem as described in Section 4.2.1 and illustrated in Figure 4-8 is the source of these low values. The results of these realizations are omitted when the final distributions for φ_m and c_m are calculated. The final obtained distributions of $E_{m\ 32\ MPa}$, $v_{m\ 32\ MPa}$, $E_{m\ 8\ MPa}$, $v_{m\ 8\ MPa}$, φ_m and c_m are summarized in Table 4-3 for rock domain B. The distributions of parameters that are given in this table only account for the influence of variation in the fracture pattern on the rock mass properties (as input mechanical parameters are constant).

4.2.4 Summary of DFN geometry-induced rock mass variability

The results from all the 3DEC simulations on DFN-realizations for Rock Domain A and B are plotted in Figure 4-23 and Figure 4-24. These illustrate respectively the variation of the rock mass deformation modulus with confining stress and the major and minor stress at failure at the different stress levels. The difference between Rock Domain A and B is not significant. The spread is maybe a little larger in Rock Domain B.
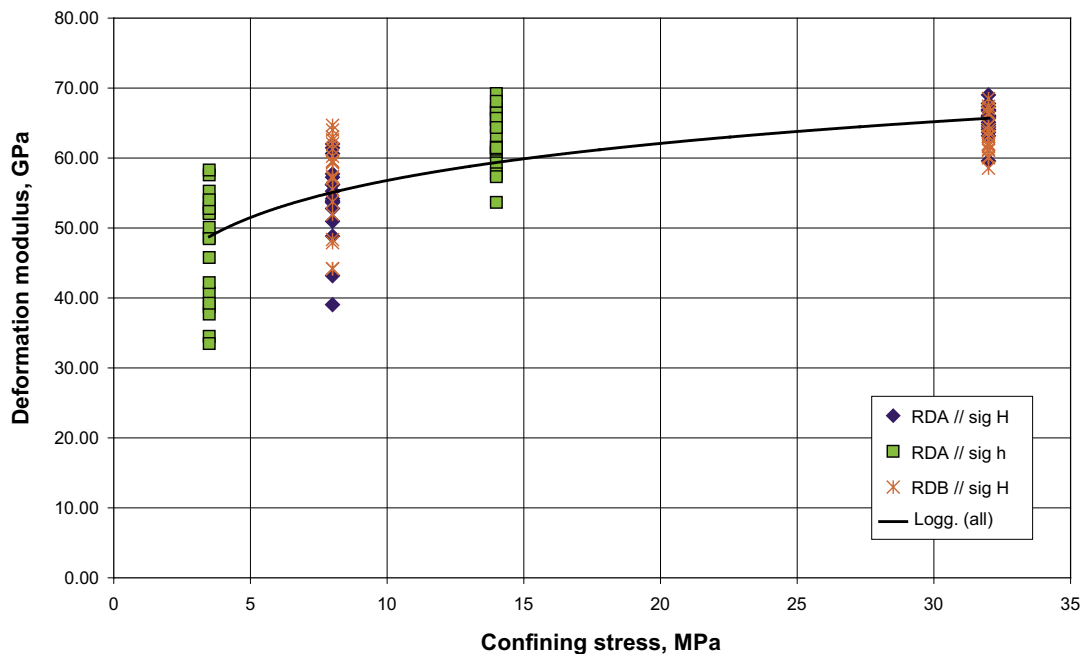
***Figure 4-23.** Variation of the deformation modulus as a function of confining stress.*
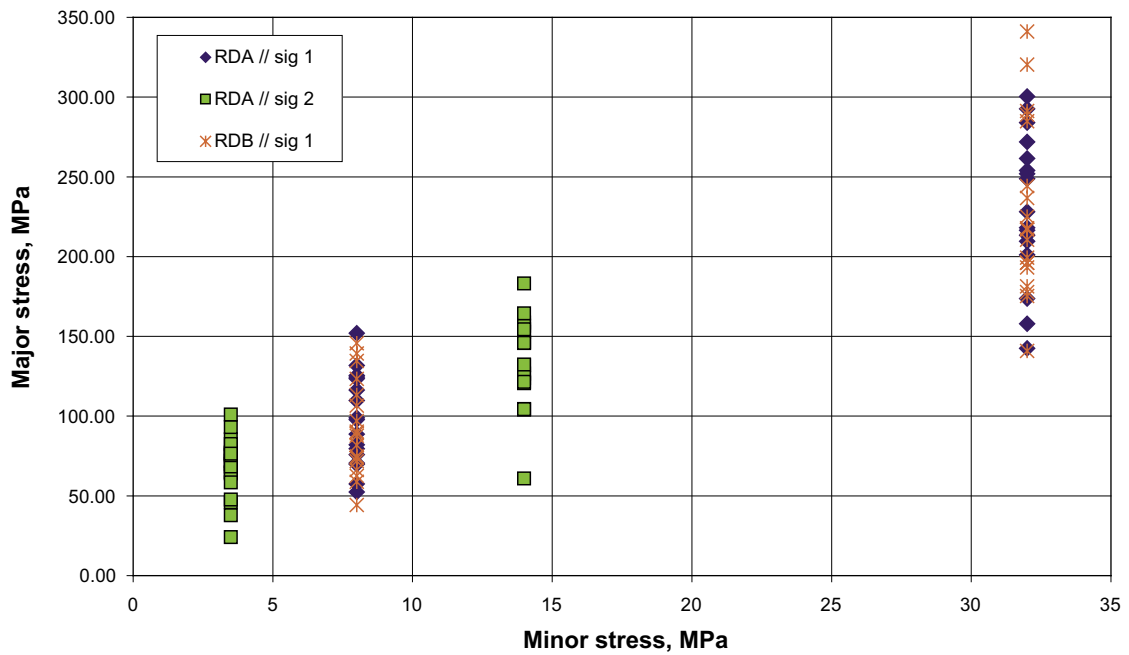
Figure 4-24. *Major and minor principle stresses at failure in the rock mass.*

Based on these observations the simulations for DFN-realizations parallel to σ_2 in Rock Domain B have been omitted as similar results as for rock domain A are expected.

Figure 4-23 illustrates a dependency of the deformation modulus with confining stress. Whatever the rock domain and the orientation of the trace planes the deformation modulus increases with confining stress up to a constant value reaches above about 15 MPa confining stress. However the deformation modulus does not appear to be dependent on to the orientation of the DFN trace planes orientations, which can be explained by an almost isotropic DFN model.

Therefore with consideration to time constraints the influence of variation of input parameters has only been analyzed for the trace planes parallel to σ_H in rock domains A and B.

4.3 Material property influence on rock mass parameters

Next, the input material property influence on rock mass parameters is estimated as independent components.

The material property influence on rock mass parameters has been evaluated for simulations parallel to σ_H in rock domain A and B. Similarly to Section 4.1, the two confining pressures 32 MPa and 8 MPa are used to estimate the influence that individual material parameters have on $E_{m\ 32\ MPa}$, $v_{m\ 32\ MPa}$, $E_{m\ 8\ MPa}$, $v_{m\ 8\ MPa}$, φ_m and c_m. This is done by performing 3DEC-simulations on a specific "average" realization (here realization 14 for the two rock domains), where each material property, one-by-one, is assigned its minimum and its maximum value, while all other material properties are set to their mean values (Table 3-1). Relationships can then be established between variations in all input material parameters and their respective impact on rock mass properties.

As a start all relationships between input material properties and rock mass properties are assumed linear and independent, i.e. can be approximated by separate proportionality constants k_{X_i,Y_m}, where X_i is an input property (intact rock or fractures) and Y_m is a resulting rock mass parameter. The rock mass properties are evaluated for three different values of each input property: its minimum, mean, and maximum value. Thus, two proportionality constants can be achieved, one for cases when the input property is less than its mean (Equation 4.1) and one when the input property is larger than its mean (Equation 4.2):

$$k_{X_i,Y_m}\left(X_i < X_{i,0} \right) = \frac{Y_m - Y_{m,0}}{X_{i,\min} - X_{i,0}} \tag{4.1}$$

and

$$k_{X_i,Y_m}\left(X_i > X_{i,0} \right) = \frac{Y_m - Y_{m,0}}{X_{i,\max} - X_{i,0}} \tag{4.2}$$

where $X_{i,\min}$, $X_{i,0}$, and $X_{i,\max}$ are the minimum, mean and maximum input parameter values, respectively, and Y_m and $Y_{m,0}$ are the resulting rock mass parameters calculated with 3DEC.

As an example, the influence that the deformation modulus of intact rock, E_i, has on the deformation modulus of rock mass, E_m, is shown in Figure 4-25. 3DEC simulations with E_i set to its minimum, mean and maximum values (all other parameters set to their mean values), provide three corresponding values of E_m. Two proportionality constants $k_{Ei,Em}$ ($E_i < E_{i,0}$) and $k_{Ei,Em}$ ($E_i > E_{i,0}$) are then evaluated; these are found to be in this case 0.581 and 0.548, respectively.

The influences of all input parameters on rock mass properties are summarized in Table 4-4 and Table 4-5, and as can be noted, some proportionality constants may change sign depending on if its input parameter value is above or below its mean. Note that, since the units of the various proportionality constants are mixed, a direct comparison of their relative magnitudes may be misleading.
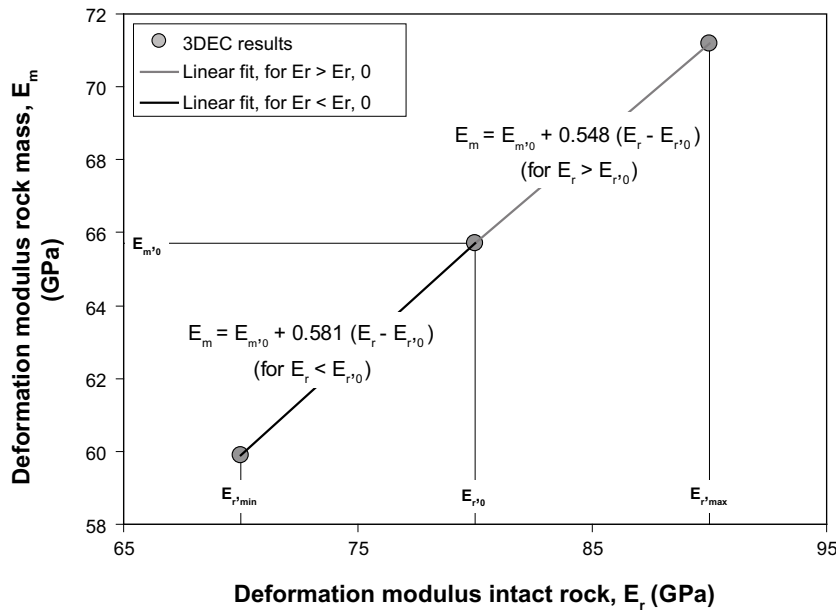
Figure 4-25. *Evaluation of the influence the deformation modulus of intact rock, E_i, has on the deformation modulus of rock mass, E_m, in Rock Domain A for confinement 32 MPa.*

Table 4-4. Dependency of rock mass parameters on input parameters set above the mean value, proportionality constant $k_{Xi,Ym}$.

		Confinement 32 MPa		Confinement 8 MPa		Rock mass stength	
		$E_{m\,32\,MPa}$ (GPa)	$v_{m\,32\,MPa}$ (−)	$E_{m\,8\,MPa}$ (GPa)	$v_{m\,8\,MPa}$ (−)	c_m (MPa)	φ_m (°)
RDA, intact rock	E_i (GPa)	0.55	0	1.26	−0.01	0.24	−0.12
	v_i (−)	−21.42	0.68	28.87	0.3	29.83	−5.65
	c_i (MPa)	0.01	0	0.52	−4.E−03	0.69	−0.31
	T_i (MPa)	5.E−03	−3.E−06	0.01	2.E−05	0.42	−0.21
	φ_i (°)	0.01	−6.E−06	0.03	1.E−04	1.	−0.56
RDA, Fractures	K_n (MPa/mm)	0.01	2.E−04	0.09	−7.E−04	0.02	−0.01
	K_s (MPa/mm)	0.09	−4.E−04	0.3	−4.E−03	0.19	−0.16
	φ_f (°)	0.12	−6.E−04	0.6	−5.E−03	0.08	0.37
	c_f (MPa)	0.13	−3.E−03	0.2	−0.02	1.03	−0.01
RDB, intact rock	E_i (GPa)	0.62	0	0.36	3.E−04	0.07	0.01
	v_i (−)	−0.86	0.66	165.33	−0.12	58.4	−21.8
	c_i (MPa)	3.E−03	6.E−06	3.E−04	−2.E−06	0.83	−0.24
	T_i (MPa)	0.01	2.E−05	0.E+00	0.E+00	0.29	−0.16
	φ_i (°)	0.01	2.E−07	−3.E−04	8.E−07	−0.43	0.61
RDB, Fractures	K_n (MPa/mm)	0.04	3.E−04	0.02	3.E−04	−0.01	−0.01
	K_s (MPa/mm)	0.1	−5.E−04	0.13	2.E−05	0.04	−0.02
	φ_f (°)	0.03	−2.E−04	0.34	−2.E−03	−0.44	0.73
	c_f (MPa)	0.25	−3.E−04	0.21	−8.E−04	1.45	−0.29

Table 4-5. Dependency of rock mass parameters on input parameters set below the mean value, proportionality constant $k_{Xi,Ym}$.

		Confinement 32 MPa		Confinement 8 MPa		Rock mass stength	
		$E_{m\,32\,MPa}$ (GPa)	$v_{m\,32\,MPa}$ (−)	$E_{m\,8\,MPa}$ (GPa)	$v_{m\,8\,MPa}$ (−)	c_m (MPa)	φ_m (°)
RDA, intact rock	E_i (GPa)	0.58	3.E−04	0.66	2.E−03	−0.18	0.19
	v_i (−)	−1.46	0.83	11.94	0.13	4.8	1.23
	c_i (MPa)	0.01	0.E+00	−0.78	0.01	−0.19	0.18
	T_i (MPa)	−0.01	4.E−06	−0.01	−2.E−05	−0.54	0.27
	φ_i (°)	−0.02	−4.E−06	−0.03	4.E−07	−0.72	0.53
RDA, Fractures	K_n (MPa/mm)	0.07	6.E−04	0.05	5.E−04	−0.04	0.03
	K_s (MPa/mm)	0.6	−2.E−03	−0.22	1.E−03	−0.03	0.05
	φ_f (°)	0.5	−3.E−03	0.73	−4.E−03	−0.62	0.85
	c_f (MPa)	0.3	−6.E−04	4.03	−0.01	−3.08	0.4
RDB, intact rock	E_i (GPa)	0.63	5.E−05	0.52	−6.E−05	0.2	−0.14
	v_i (−)	2.77	0.88	−83.05	1.54	9.71	6.29
	c_i (MPa)	−4.E−03	−2.E−05	4.E−03	−2.E−05	0.26	0.04
	T_i (MPa)	−0.01	−1.E−05	3.E−03	−1.E−05	−0.54	0.25
	φ_i (°)	1.E−03	−2.E−05	5.E−03	−3.E−05	0.18	0.18
RDB, Fractures	K_n (MPa/mm)	0.14	6.E−04	0.13	6.E−04	−0.02	−0.01
	K_s (MPa/mm)	0.46	−2.E−03	−0.04	−2.E−04	0.	0.03
	φ_f (°)	−0.16	−3.E−04	0.81	−4.E−03	−0.01	0.22
	c_f (MPa)	−0.21	−0.01	2.46	−0.01	−3.35	3.88

4.4   Monte-Carlo simulations

The total range of rock mass parameter variability in $E_{m\ 32\ MPa}$, $\nu_{m\ 32\ MPa}$, $E_{m\ 8\ MPa}$, $\nu_{m\ 8\ MPa}$, φ_m and c_m is finally estimated using a Monte-Carlo based GoldSim model. This is done by combining the two following distributions:

1. One distribution which accounts only for the variation of the fracture pattern by means of DFN realisations run in 3DEC, see Section 4.2.1 and 4.2.3, and

2. One distribution which accounts for the variation of the input mechanical parameters in the 3DEC simulations, see Section 4.3. This distribution was obtained from 3DEC simulations on one DFN realisation. The influence of the variation of the input mechanical parameters is assumed to be similar for all DFN realisations.

The procedure for simulations is the following:

• One random value is extracted from the distribution which describes the influence of the variation of the fracture pattern.

• A random value extracted from the distribution accounting for the variation of input mechanical parameters is added to the precedent value.

• 100,000 random values are produced from both distributions and the resulting properties are statistically analysed. The distribution of the rock mass properties is illustrated in Figure 4-28 to Figure 4-28 for rock domains A and B.
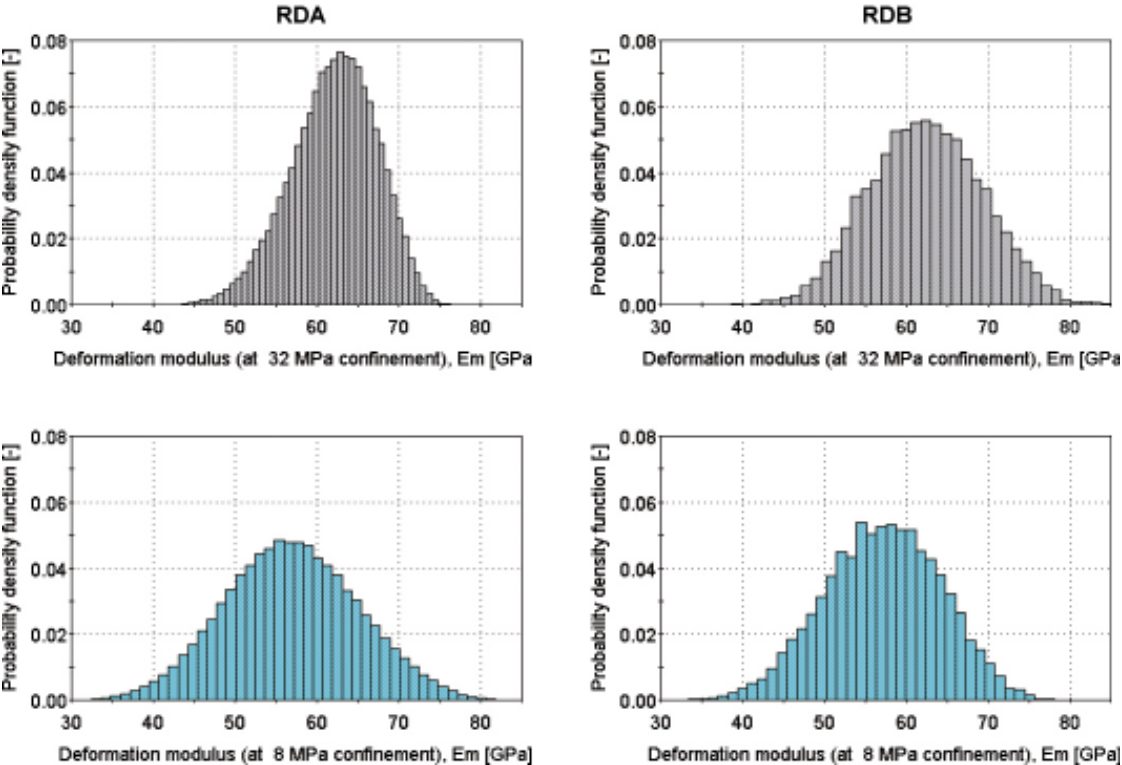
Figure 4-26. *Probability density function of Deformation modulus is Rock Domain A and B.*
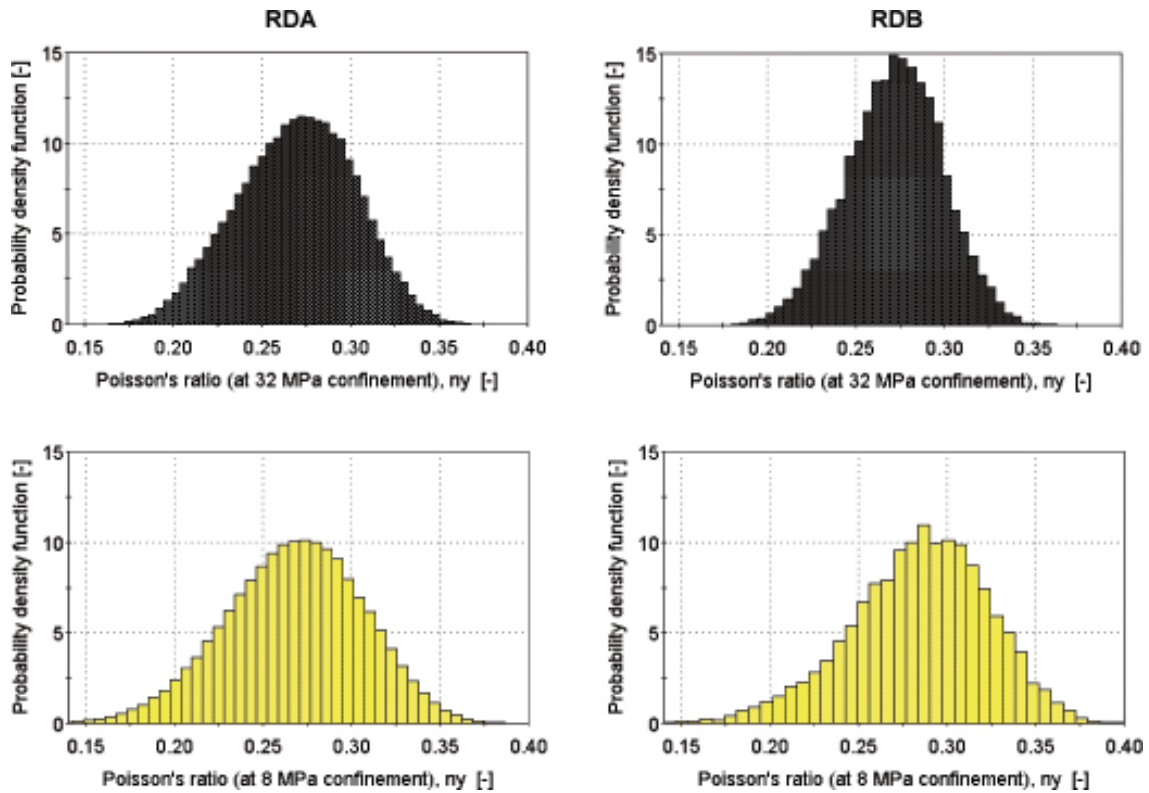
Figure 4-27. *Probability density function of Poisson's ratio in Rock Domain A and B.*

The obtained distributions of UCS_m, c_m and φ_m are also shown as probability distributions of simulated triaxial loading tests in Figure 4-29. As can be seen, the lower limit of UCS_m is 55 MPa for RDA and 5 MPa for RDB.

The covariance matrices in Table 4-6 and Table 4-7 indicate that E_m depends strongly on the deformation modulus of the intact rock, E_r, and on the four fracture properties; most strongly on fracture shear stiffness, K_s. Similarly, the Poisson's ratio of the rock mass, ν_m, depends strongly on Poisson's ratio of intact rock, ν_r, and also on the four fracture properties. The friction angle of the rock mass, φ_m, is positively correlated to the friction angle of intact rock, φ_r, and that of fractures, φ_f, while it is negatively correlated to c_r and c_f. The opposite holds for the cohesion of the rock mass c_m. However, the parameter T_r seems to be of little significance to any of the examined rock mass parameters. The uniaxial compressive strength of the rock mass, UCS_m, is strongly correlated to the cohesion of the intact rock in RDB, while this correlation is much weaker for RDA. This can be explained by the larger fracture intensity in RDB, which implies that UCS_m is largely determined by DFN geometry-induced variability (pattern and intensity) and hence the correlations to input property parameters are suppressed.
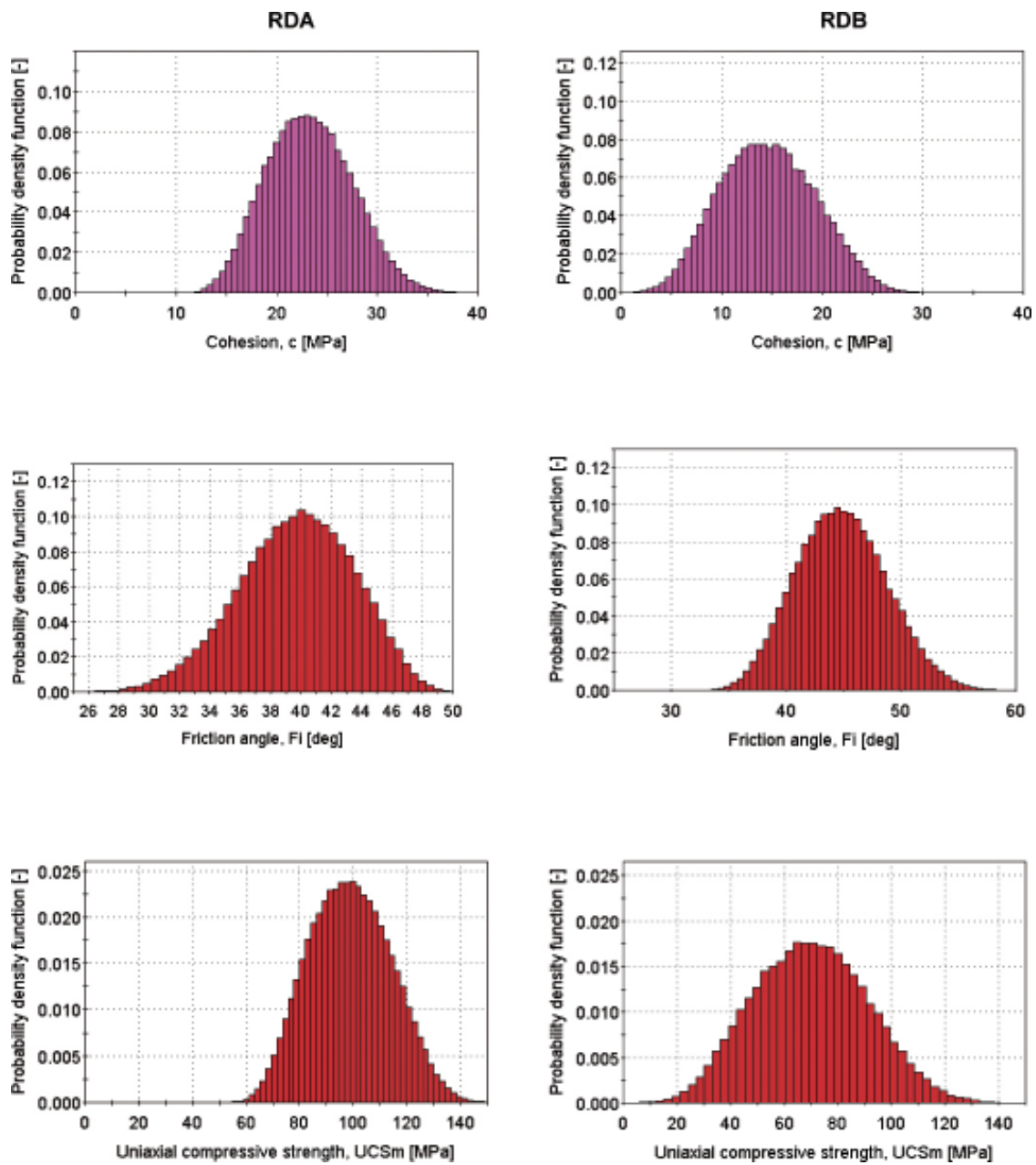
Figure 4-28. *Probability density function of the rock mass mechanical properties in Rock Domain A and B (accounting for variation in fracture pattern and input parameters)*
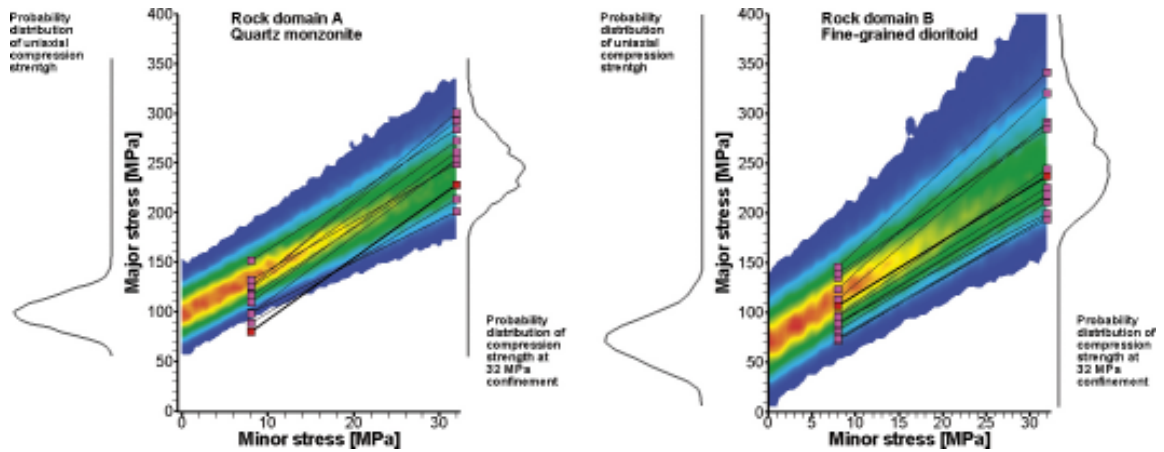
Figure 4-29. *Probability distributions of simulated triaxial test for rock mass of RDA and RDB. Pink boxes are results from 3DEC modelling of different DFN realizations at confining stress levels 8 MPa and 32 MPa. Red boxes refer to the realization that was used to evaluate the influence that various input parameters have on rock mass properties.*

Table 4-6. Correlation coefficient matrix between rock mass parameters and input parameters, RDA.

	Confinement 32 MPa		Confinement 8 MPa				
	E_m	v_m	E_m	v_m	c_m	φ_m	UCS_m
E_i	**0.59**	0.01	**0.64**	−0.26	0.02	0.05	0.05
v_i	−0.08	**0.82**	0.08	0.18	0.14	−0.01	0.16
c_i	0.01	0.00	0.05	−0.09	**0.34**	**−0.18**	**0.30**
φ_i	0.00	0.00	−0.01	0.04	**−0.15**	**0.13**	−0.11
T_i	0.00	0.01	0.00	0.00	0.02	−0.01	0.02
K_n	**0.18**	**0.29**	0.24	−0.10	−0.04	0.02	−0.03
K_s	**0.60**	**−0.34**	0.04	−0.32	0.16	−0.14	0.11
c_f	−0.14	0.10	−0.18	0.19	0.16	**−0.40**	−0.04
φ_f	0.22	−0.18	**0.32**	**−0.40**	−0.26	**0.60**	0.04

Table 4-7. Correlation coefficient matrix between rock mass parameters and input parameters, RDB.

	Confinement 32 MPa		Confinement 8 MPa				
	E_m	v_m	E_m	v_m	c_m	φ_m	UCS_m
E_i	**0.78**	−0.01	**0.51**	0.04	0.20	−0.10	0.19
v_i	−0.01	**0.74**	0.09	**0.56**	0.18	−0.04	0.18
c_i	0.01	0.00	−0.01	0.01	**0.72**	**−0.28**	**0.67**
φ_i	0.00	0.00	0.01	0.00	**−0.19**	**0.36**	−0.08
T_i	0.01	0.01	0.00	0.01	−0.06	0.03	−0.06
K_n	**0.33**	**0.43**	0.25	0.30	−0.06	−0.08	−0.09
Ks	**0.37**	**−0.42**	0.05	−0.04	0.04	0.01	0.04
cf	0.03	0.01	−0.19	0.19	0.13	**−0.28**	0.06
φf	−0.03	−0.04	**0.31**	**−0.32**	**−0.22**	**0.49**	−0.08

4.4.1 Adjusting boundaries

The results in the previous section rely on the assumption that all sources of variability on the rock mass parameters are linear and independent. In order to examine this assumption, the input parameter combinations that yield the maximum and minimum UCS_m values were examined for both domains. These extreme parameter combinations were modeled with 3DEC and were also used in GoldSim. The values obtained are summarized and compared in Table 4-8. As can be seen, the results of Monte-Carlo simulations indicate that the "best" parameter combination increases UCS_m by 74.7 MPa for RDA, while the "worst" combination decreases UCS_m by 2.6 MPa. Quite contradictory, the "best" combination decreases by 5.5 MPa, as evaluated by 3DEC. For RDB, Monte-Carlo simulations and 3DEC modeling seem to provide more consistent results, although the range of variation is smaller for the 3DEC values.

A conclusion is that the assumption of linear independency exaggerates the impact that variable input parameters have on rock mass compressive strength, at least for the specific extreme combinations that have been "validated" with 3DEC. The values of φ_m and UCS_m that were obtained for the extreme combinations are also shown as compressive strengths for a triaxial loading experiment in Figure 4-30.

In order to remove this exaggeration of the Monte-Carlo simulations, these were re-run such that the predicted impact on φ_m and UCS_m were rescaled according to the "maximum" and "minimum" limits determined by 3DEC. The values presented as Probability Density Function are illustrated in Figure 4-31.

The values obtained for UCS_m are plotted as results of simulated triaxial loading tests. Figure 4-32 illustrates the variation related to the fracture pattern and Figure 4-33 the relation impeded to the variation of input parameters.

Table 4-8. Input parameter combinations that yield maximum influence on UCS_m.

	E_i	v_i	c_i	φ_i	T_i	k_n	k_s	c_f	φ_f	ΔUCS_m, GoldSim	ΔUCS_m, 3DEC
RDA											
Best	max	max	max	min	max	min	max	high	max		
	90	0.33	29	57	24	49	49	0.69	40	74.7	−5.5
Worst	avg	min	avg	avg	avg	avg	avg	avg	avg		
	80	0.18	20	60	17	100	29	0.50	32	−2.6	−1.28
RDB											
Best	max	max	high	avg	low	min	max	high	max		
	110	0.31	40	55	24	49	49	0.73	40	68.5	29.4
Worst	min	min	min	max	min	max	min	min	max		
	70	0.19	20	60	20	179	10	0.065	40	−58.3	−3.1

Max, min and avg refer to the minimum, maximum and average value of the input parameter.
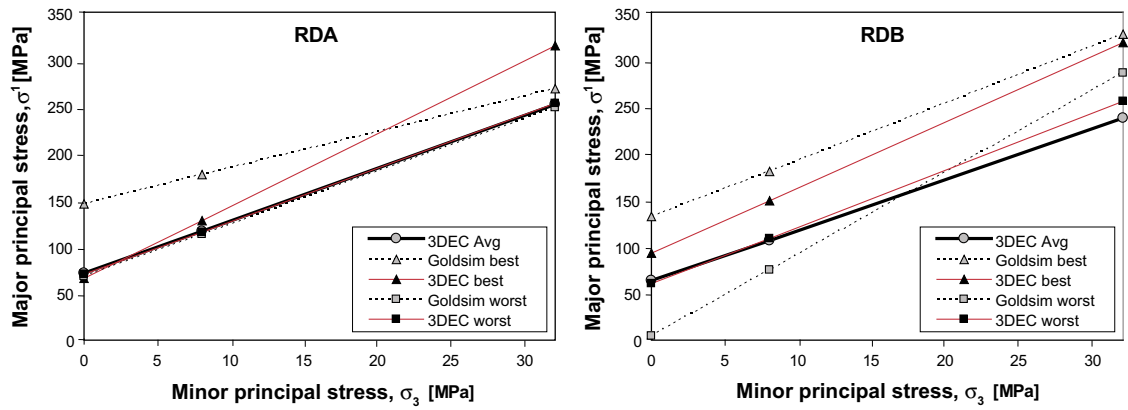
Figure 4-30. *φ_m and UCS_m for extreme cases of input parameter combinations, shown as a triaxial test for rock mass, rock domains A and B.*
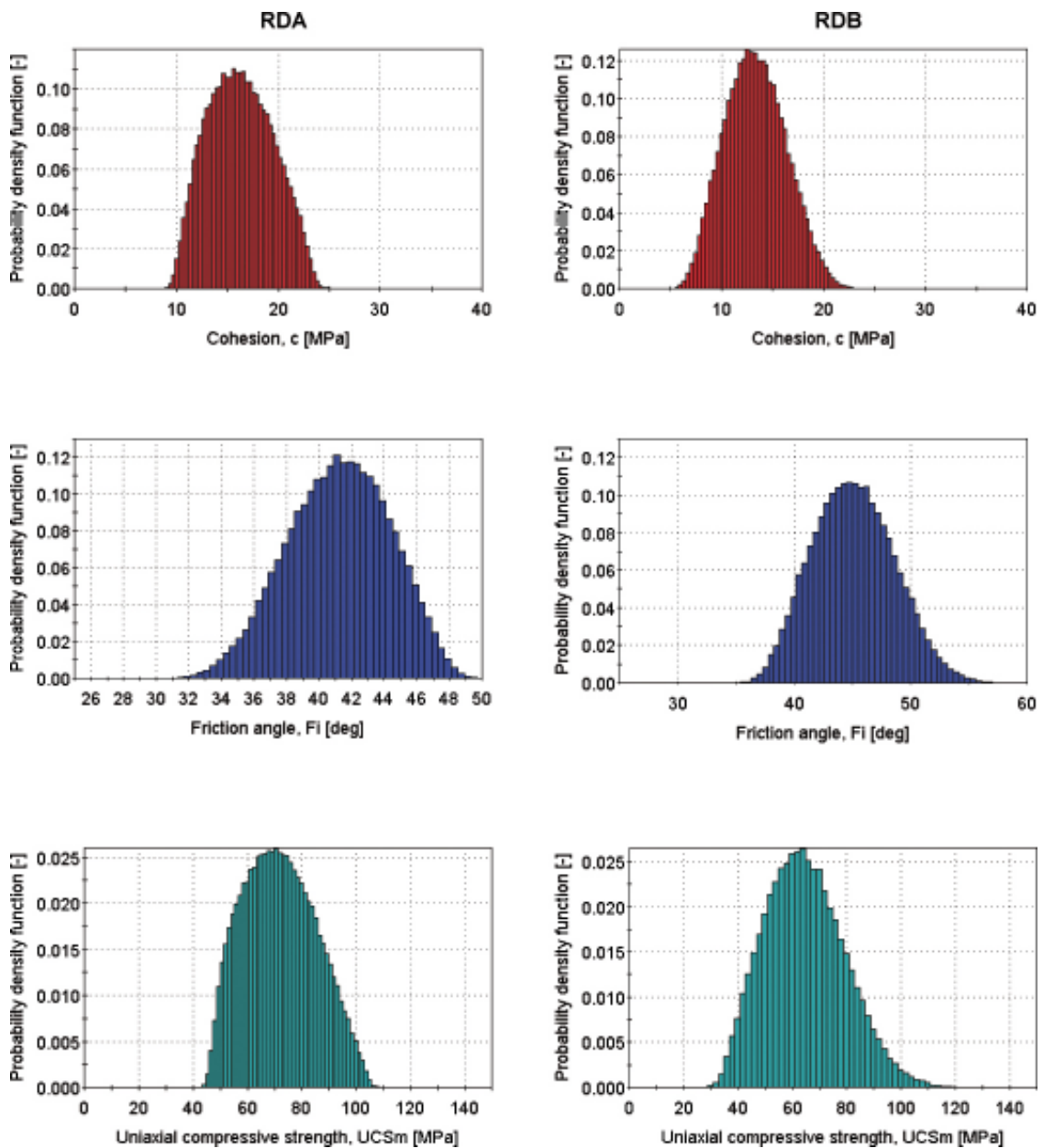
Figure 4-31. *Probability density function of cohesion, friction angle and unixial compressive strength of the rock mass, Rock Domains A and B.*
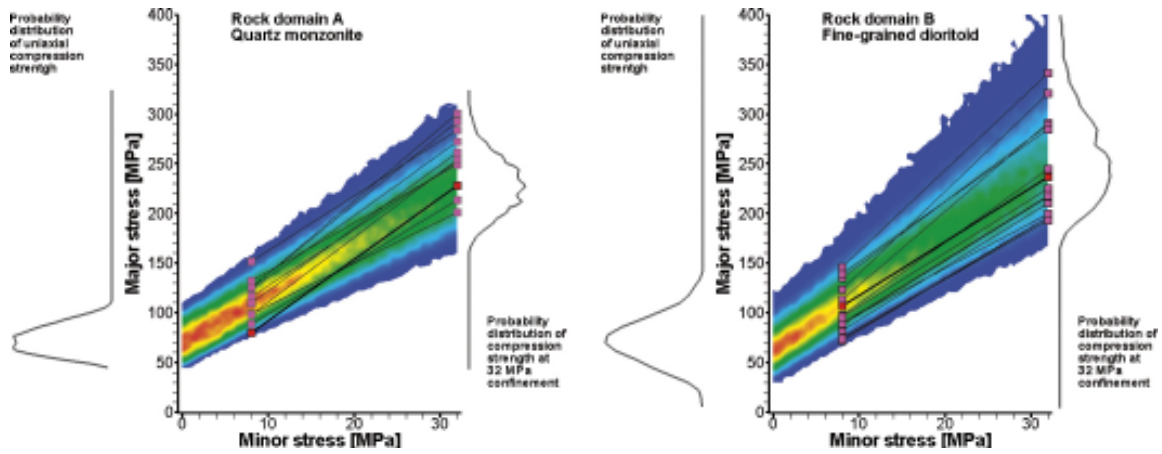
Figure 4-32. *Probability distributions of simulated triaxial test for rock mass of RDA and RDB. Pink boxes are results from 3DEC modelling of different DFN realizations at confining stress levels 8 MPa and 32 MPa. Red boxes refer to the realization that was used to evaluate the influence that various input parameters have on rock mass properties.*
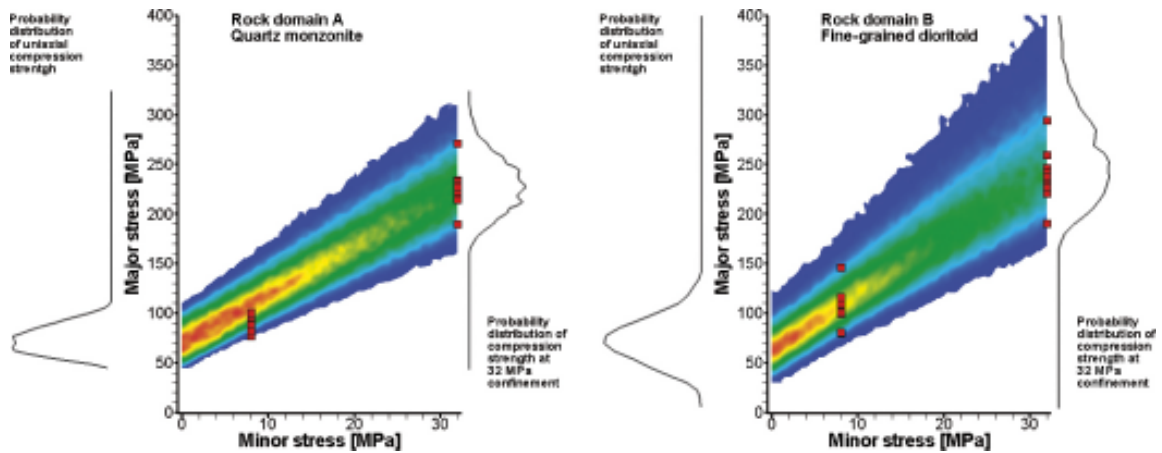
Figure 4-33. *Probability distributions of simulated triaxial test for rock mass of RDA and RDB. Red boxes are results from 3DEC modelling on one DFN realization at confing stress levels 8 and 32 MPa, when one input property at a time was set to its maximum or minimum value, while all other parameters were kept at their respective mean values.*

4.4.2 Combined results

The distribution of the predicted rock mass mechanical properties is given in Table 4-9 for rock domain A and B. These values account for both the influence of the fracture pattern and the influence of the variation of input property parameters.

Table 4-9. Distribution of the predicted rock mass mechanical properties, rock domain A and B.

Parameter for the rock mass (20×20×20 m scale)	Rock Domain *A* Truncated normal distribution mean/standard dev.	Rock Domain *A* Min trunc. – max trunc	Rock Domain B Truncated normal distribution mean/standard dev.	Rock Domain B Min trunc. – max trunc
Deformation Modulus	59 GPa/8 GPa[2] 62 GPa/5 GPa[3]	36–82 GPa 45–75 GPa	57 GPa/7 GPa[2] 62 GPa/7 GPa[3]	36–76 GPa 42–82 GPa
Poisson's ratio	0.25/0.04[2] 0.27/0.03[3]	0.11–0.36 0.17–0.32	0.28/0.04[2] 0.27/0.03[3]	0.15–0.38 0.19–0.35
Tensile strength	0 MPa		0 MPa	
Before adjusting maximum impact of extreme input parameter combination to 3DEC results				
Uniaxial compressive strength[1]	99 MPa/15.3 MPa	60–143 MPa	70 MPa/21 MPa	14–133 MPa
Mohr-Coulomb, φ_m	40°/3.8°	28°–49°	44°/3.9°	35°–57°
Mohr-Coulomb, c_m[4]	23.3/4.2 (–0.5421)	12–36	14.6/4.7 (–0.3729)	2.6–28
After adjusting maximum impact of extreme input parameter combination to 3DEC results				
Uniaxial compressive strength[1]	72 MPa/13.4 MPa	45–105 MPa	65 MPa/14.6 MPa	32–113 MPa
Mohr-Coulomb, φ	41°/3.1°	32°–49°	45°/3.5°	36°–56°
Mohr-Coulomb, c[4]	16.3/3.2 (–0.3156)	10–24	13.3/3.0 (–0.1911)	6–22

[1] This description parameter is not a standard parameter, it refers to the strength of a block of 30 m size with low confinement at boundaries.

[2] For confining stress, 8 MPa and lower.

[3] For confining stress, 32 MPa.

[4] The cohesion is correlated to the friction angle. The friction angle given in ° and the correlation coefficient is specified within brackets.

5   Discussion

Assumption of linear independency could be tested with additional 3DEC simulations, where more than one property is varied at a time. The boundary adjustment in Section 4.4.1 is undertaken for the parameter combinations that produce the extreme cases of impact on UCS_m. These combinations are themselves determined under assumption of linear independency, and consequently do not guarantee that other, more extreme, combinations does not exist. In coming analyses it might be more appropriate to run more simulations with 3DEC for different parameter combinations to get the material property influence on the rock mass parameters.

Stochastic variability in fracture properties among fractures in DFN realizations have not been examined, because of limitations in 3DEC. Instead, all fractures within a DFN realization have been assigned the same values: either their minimum, mean or maximum parameter values, which seems unrealistic. It is also difficult to tell whether this simplification exaggerates or underestimates the fracture input parameter variability impact on rock mass properties. However some tests were conducted during the development of the modeling strategy on the influence of fracture parameters for different fracture sets. The results are presented in /Olofsson and Fredriksson 2005/.

The DFN-induced variability component is only evaluated for a limited number of realizations ($n \leq 17$ for RDA and $n \leq 19$ for RDB).

The influences of input parameters on rock mass properties have only been examined for one DFN realization of RDA and one for RDB. The influence in rock mass properties from material properties of intact rock and fractures should be tested using a few other realizations in order to evaluate their potential similarity in behavior.

The most important limitation in the description of variability is that the analyses presented in this report are based only on the mean values of the fracture intensity. No variability of the fracture intensity inside a rock domain was tested although the fracture intensity in Simpevarp is shown to vary quite significantly. Therefore the influence of fracture intensity should be analyzed in detail in coming modeling stages.

6   Conclusions

The rock mass mechanical properties have been determined by means of numerical modelling. The modelling is carried out in 3DEC and the block model is built using the fracture network described by the site specific DFN model.

The data uncertainty and variability is studied in two steps, first by analysing the influence of the fracture pattern, and then by studying the influence of the variation of the input parameters. Their combined effect is analysed by means of Monte-Carlo simulations.

The rock mass properties were determined for each rock domain. The rock domains are characterised by their structure and lithologies and as such the fracture network might be different. However the geological description of the four rock domains illustrates that rock types and fracture characteristics in rock domains C and D do not significantly differ from the properties observed in rock domain A. Hence only rock domains A and B were analysed in this study (and the estimated rock mass mechanical properties of rock domains A and D are derived from those estimated for rock domain A).

Table 6-1 and Table 6-2 present the distribution of the predicted rock mass mechanical properties for the four rock domains identified in Simpevarp.

Table 6-1. Predicted rock mechanical properties for the mass, rock domain A and B.

Parameter for the rock mass (20×20×20 m scale)	Rock Domain *A* Truncated normal distribution mean/standard dev.	Rock Domain *A* Min trunc. – max trunc	Rock Domain B Truncated normal distribution mean/standard dev.	Rock Domain B Min trunc. – max trunc
Uniaxial compressive strength[1]	72 MPa/13.4 MPa	45–105 MPa	65 MPa/14.6 MPa	32–113 MPa
Deformation Modulus	59 GPa/8 Gpa[2] 62 Gpa/5 GPa[3]	36–82 GPa 45–75 GPa	57 GPa/7 GPa[2] 62 GPa/7 GPa[3]	36–76 GPa 42–82 GPa
Poisson's ratio	0.25/0.04[2] 0.27/0.03[3]	0.11–0.36 0.17–0.32	0.28/0.04[2] 0.27/0.03[3]	0.15–0.38 0.19–0.35
Tensile strength	0 MPa		0 MPa	
Mohr–Coulomb, φ_m	41°/3.1°	32°–49°	45°/3.5°	36°–56°
Mohr–Coulomb, c_m[4]	16.3/3.2 (–0.3156)[4]	10–24	13.3/3.0 (–0.1911)[4]	6–22

[1] This desription parameter is not a standard parameter, it refers to the strength of a block of 20 m size with low confinement at boundaries.

[2] For confining stress, 8 MPa and lower.

[3] For confining stress, 32 MPa.

[4] The cohesion and the friction angle are correlated. The correlation coefficient is specified within brackets.

Table 6-2. Predicted rock mechanical properties for the mass, rock domain C and D.

Parameter for the rock mass (20×20×20 m scale)	Rock Domain *C* Truncated normal distribution mean/standard dev.	Rock Domain *C* Min trunc. – max trunc	Rock Domain D Truncated normal distribution mean/standard dev.	Rock Domain D Min trunc. – max trunk
Uniaxial compressive strength[1]	72 MPa/13.4 MPa	45–105 MPa	72 MPa/13.4 MPa	45–105 MPa
Deformation Modulus	59 GPa/8 GPa[2] 62 GPa/5 GPa[3]	36–82 GPa 45–75 GPa	59 GPa/8 GPa[2] 62 GPa/5 GPa[3]	36–82 GPa 45–75 GPa
Poisson's ratio	0.25/0.04[2] 0.27/0.03[3]	0.11–0.36 0.17–0.32	0.25/0.04[2] 0.27/0.03[3]	0.11–0.36 0.17–0.32
Tensile strength	0 MPa		0 MPa	
Mohr-Coulomb, φ_m	41°/3.1°	32°–49°	41°/3.1°	32°–49°
Mohr-Coulomb, c_m[4]	16.3/3.2 (–0.3156)[4]	10–24	16.3/3.2 (–0.3156)[4]	10–24

[1] This desription parameter is not a standard parameter, it refers to the strength of a block of 20 m size with low confinement at boundaries.

[2] For confining stress, 8 MPa and lower.

[3] For confining stress, 32 MPa.

[4] The cohesion and the friction angle are correlated. The correlation coefficient is specified within brackets.

7   References

3DEC, 2003. 3 Dimensional Distinct Element Code, User's Guide. Itasca consulting group Inc., Minneapolis.

Hakami E, Min K-B, 2005. Modelling of the state of stress. Preliminary site description, Simpevarp subarea – version 1.2. SKB R-05-19, Svensk Kärnbränslehantering AB.

Lanaro F, Fredriksson A, 2005. Rock mechanics characterisation of the rock mass – Sumamry of primary data. Preliminary site description, Simpevarp subarea – version 1.2. SKB R-05-21, Svensk Kärnbränslehantering AB.

LaPointe P R, Hermanson J, 2005. Statistical model for fractures and deformation zones, Simpevarp 1.2. In progress, SKB R-05-28, Svensk Kärnbränslehantering AB.

Olofsson I, Fredriksson F, 2005. Strategy for a numerical Rock Mechanics Site Descriptive Model. Further development of the theoretical/numerical approach. SKB R-05-43, Svensk Kärnbränslehantering AB.

SKB, 2005. Preliminary Site Description. Simpevarp subarea – version 1.2. SKB R-05-08, Svensk Kärnbränslehantering AB.

Table A-1. Poisson's ratio, deformation modulus and vertical stress at failure for all DFN realisations, trace planes parallel to σ_H, high stress level (32.0 MPa), Rock Domain A.

DFN realisation	Poisson's ratio, v_m	Deformation modulus, E_m, GPa	Vertical stress at failure, σ_{vf}, MPa
1	0.28	67.82	271.89
2	0.27	64.43	209.58
3	0.26	65.93	213.38
4	0.26	66.10	216.52
5	0.27	65.11	284.05
7	0.29	63.67	251.90
8	0.27	64.10	173.66
9	0.25	59.59	201.08
10	0.27	66.91	261.59
11	0.27	67.35	142.51
12	0.27	69.01	248.84
13	0.30	66.90	218.14
14	0.28	65.71	228.09
17	0.27	66.72	254.06
18	0.28	63.18	300.45
19	0.28	65.96	292.58
20	0.27	64.77	157.86
Mean	**0.27**	**65.49**	**230.95**
Standard dev.	**0.01**	**2.16**	**45.99**
Min.	**0.25**	**59.59**	**142.51**
Max.	**0.30**	**69.01**	**300.45**

Table A-2. Poisson's ratio, deformation modulus and vertical stress at failure for all DFN realisations, trace planes parallel to σ_H, low stress level (8.0 MPa), Rock Domain A.

DFN realisation	Poisson's ratio, v_m	Deformation modulus, E_m, GPa	Vertical stress at failure, σ_{vf}, MPa
1	0.34	53.79	123.50
2	0.34	48.83	70.59
3	0.33	52.78	88.68
4	0.30	53.88	82.08
5	0.30	56.19	151.96
7	0.32	55.27	116.37
8	0.37	39.05	69.87
9	0.28	57.72	99.00
10	0.28	62.03	109.79
11	0.37	43.17	57.47
12	0.33	53.62	131.70
13	0.35	50.97	75.90
14	0.33	57.27	79.61
17	0.31	60.66	97.78
18	0.32	54.20	124.47
19	0.33	56.21	125.41
20	0.29	61.48	52.44
Mean	**0.32**	**53.95**	**97.45**
Standard dev.	**0.03**	**6.01**	**28.56**
Min.	**0.28**	**39.05**	**52.44**
Max.	**0.37**	**62.03**	**151.96**

Table A-3. Friction angle, cohesion and uniaxial compressive strength for all DFN realisations, trace planes parallel to σ_H, Rock Domanin A.

DFN realisation	Friction angle, φ_m	Cohesion, c_m, MPa	Uniaxial compressive strength, MPa
1	46.18	14.89	74.04
2	44.87	5.04	24.26
3	42.63	10.33	47.11
4	44.19	7.87	37.27
5	43.83	23.00	107.94
7	44.36	14.98	71.19
8	38.64	8.48	35.27
9	38.26	15.75	64.98
10	46.63	11.77	59.18
11	34.04	7.74	29.13
12	41.29	20.97	92.66
13	45.34	5.85	28.48
14	46.20	6.05	30.12
17	47.20	8.95	45.68
18	49.46	12.15	65.81
19	48.50	13.20	69.69
20	38.99	4.13	17.30
Mean	**43.56**	**11.24**	**52.95**
Standard dev.	**4.12**	**5.41**	**25.54**
Min.	**34.04**	**4.13**	**17.30**
Max.	**49.46**	**23.00**	**107.94**

Table B-1. Poisson's ratio, deformation modulus and vertical stress at failure for all DFN realisations, trace planes parallel to σ_h, high stress level (14.0 MPa), Rock Domain A.

DFN realisation	Poisson's ratio, v_m	Deformation modulus, E_m, GPa	Vertical stress at failure, σ_{vf}, MPa
1	0.28	69.19	120.59
2	0.27	65.45	146.48
3	0.30	60.76	158.49
4	0.28	60.78	123.72
5	0.29	64.58	156.50
7	0.28	61.56	131.77
8	0.28	59.28	126.59
9	0.26	57.72	121.40
10	0.28	57.30	60.84
11	0.28	66.79	145.66
12	0.26	67.10	152.71
13	0.28	66.48	145.85
14	0.26	65.65	104.03
15	0.28	61.23	183.10
16	0.29	61.45	164.30
17	0.31	53.64	132.20
18	0.27	63.18	154.37
19	0.30	64.34	104.37
20	0.27	68.08	104.19
Mean	**0.28**	**62.87**	**133.54**
Standard dev.	**0.01**	**4.11**	**28.04**
Min.	**0.26**	**53.64**	**60.84**
Max.	**0.31**	**69.19**	**183.10**

Table B-2. Poisson's ratio, deformation modulus and vertical stress at failure for all DFN realisations, trace planes parallel to σ_h, low stress level (3.5 MPa), Rock Domain A.

DFN realisation	Poisson's ratio, v_m	Deformation modulus, E_m, GPa	Vertical stress at failure, σ_{vf}, MPa
1	0.35	53.51	64.76
2	0.35	48.71	69.91
3	0.35	50.07	85.36
4	0.30	48.46	45.87
5	0.35	52.17	93.02
7	0.36	45.77	77.08
8	0.37	40.73	64.06
9	0.36	38.73	58.32
10	0.28	52.04	24.11
11	0.42	34.50	71.95
12	0.31	57.56	76.62
13	0.34	55.24	68.36
14	0.39	37.68	47.63
15	0.33	52.77	82.40
16	0.33	54.01	100.95
17	0.39	39.23	75.39
18	0.31	58.28	76.31
19	0.39	42.18	37.70
20	0.42	33.46	54.54
Mean	**0.35**	**47.11**	**67.07**
Standard dev.	**0.04**	**7.88**	**19.08**
Min.	**0.28**	**33.46**	**24.11**
Max.	**0.42**	**58.28**	**100.95**

Table B-3. Friction angle, cohesion and uniaxial compressive strength for all DFN realisations, trace planes parallel to σ_h, Rock Domain A.

DFN realisation	Friction angle, φ_m	Cohesion, c_m, MPa	Uniaxial compressive strength, MPa
1	43.11	10.01	46.15
2	49.36	8.22	44.39
3	48.50	11.55	60.98
4	49.67	3.66	19.92
5	45.74	14.61	71.86
7	42.68	12.89	58.85
8	45.44	8.85	43.22
9	45.61	7.61	37.30
10	33.74	3.17	11.86
11	48.64	8.94	47.38
12	49.24	9.52	51.25
13	49.58	7.83	42.53
14	43.32	6.22	28.83
15	54.21	7.89	48.84
16	45.70	16.25	79.83
17	43.47	12.14	56.45
18	49.72	9.22	50.29
19	46.71	3.07	15.47
20	40.61	8.73	37.98
Mean	**46.05**	**8.97**	**44.92**
Standard dev.	**4.45**	**3.56**	**17.61**
Min.	**33.74**	**3.07**	**11.86**
Max.	**54.21**	**16.25**	**79.83**

Table C-1. Poisson's ratio, deformation modulus and vertical stress at failure for all DFN realisations, trace planes parallel to σ_H, high stress level (32.0 MPa), Rock Domain B.

DFN realisation	Poisson's ratio, v_m	Deformation modulus, E_m, GPa	Vertical stress at failure, σ_{vf}, MPa
1	0.27	64.00	140.88
2	0.26	60.19	291.30
3	0.26	60.02	210.56
4	0.29	68.50	320.40
5	0.27	66.53	196.13
6	0.27	61.29	175.26
7	0.27	64.57	216.93
8	0.26	64.65	288.88
9	0.28	67.06	341.06
10	0.28	62.03	284.82
11	0.27	67.42	196.12
12	0.26	63.09	199.41
13	0.26	63.64	244.24
14	0.28	58.56	181.30
15	0.27	61.08	193.23
16	0.26	61.68	177.77
17	0.26	66.30	236.71
18	0.28	61.99	217.81
20	0.27	63.10	225.08
Mean	**0.27**	**63.46**	**228.31**
Standard dev.	**0.01**	**2.78**	**53.89**
Min.	**0.26**	**58.56**	**140.88**
Max.	**0.29**	**68.50**	**341.06**

Table C-2. Poisson's ratio, deformation modulus and vertical stress at failure for all DFN realisations, trace planes parallel to σ_H, low stress level (8.0 MPa), Rock Domain B.

DFN realisation	Poisson's ratio, v_m	Deformation modulus, E_m, GPa	Vertical stress at failure, σ_{vf}, MPa
1	0.27	64.67	44.28
2	0.27	57.38	113.31
3	0.25	64.01	81.77
4	0.31	62.61	123.41
5	0.35	48.35	71.77
6	0.25	59.54	62.61
7	0.31	57.09	87.67
8	0.28	60.26	134.61
9	0.30	61.28	145.68
10	0.31	55.54	139.28
11	0.29	59.33	74.72
12	0.27	63.00	90.25
13	0.32	53.74	96.93
14	0.27	62.03	58.83
15	0.35	44.20	73.69
16	0.32	47.92	66.20
17	0.29	59.59	106.63
18	0.35	44.19	89.29
20	0.32	51.93	95.71
Mean	**0.30**	**56.67**	**92.45**
Standard dev.	**0.03**	**6.54**	**28.58**
Min.	**0.25**	**44.19**	**44.28**
Max.	**0.35**	**64.67**	**145.68**

Table C-3. Friction angle, cohesion and uniaxial compressive strength for all DFN realisations, trace planes parallel to σ_H, Rock Domain B.

DFN realisation	Friction angle, φ_m	Cohesion, c_m, MPa	Uniaxial compressive strength, MPa
1	37.01	3.01	12.07
2	49.67	9.91	53.98
3	43.30	8.38	38.84
4	51.52	10.08	57.75
5	42.57	6.66	30.32
6	40.45	5.78	25.05
7	43.38	9.60	44.58
8	46.95	16.40	83.18
9	51.37	14.12	80.56
10	45.80	18.43	90.76
11	42.06	7.62	34.25
12	39.76	12.63	53.86
13	46.04	9.65	47.82
14	42.25	3.98	18.00
15	41.73	7.58	33.84
16	40.24	6.73	29.00
17	43.51	13.59	63.28
18	43.26	10.04	46.45
20	43.40	11.33	52.59
Mean	**43.91**	**9.76**	**47.17**
Standard dev.	**3.86**	**4.00**	**21.62**
Min.	**37.01**	**3.01**	**12.07**
Max	**51.52**	**18.43**	**90.76**